RSC Advances

ROYAL SOCIETY OF CHEMISTRY

www.rsc.org/advances

Study of temperature dependent three components dynamic covalent assembly via Hantzsch reaction catalyzed by dioxido- and oxidoperoxidomolybdenum(VI) complexes under solvent free condition†

Mannar R. Maurya,*[a] Neeraj Saini[a] and Fernando Avecilla[b]

[a] *Department of Chemistry, Indian Institute of Technology Roorkee, Roorkee 247 667, India. E–mail: rkmanfcy@iitr.ernet.in; Fax: +91 1332 273560; Tel: +91 1332 285327*

[b] *Departamento de Química Fundamental, Universidade da Coruña, Campus de A Zapateira, 15071 A Coruña, Spain*

Abstract

Tridentate ONO donor ligands derived from heterocyclic compound 4-acetyl-3-methyl-1-phenyl-2-pyrazoline-5-one (Hap) and aromatic hydrazides {benzoyl hydrazide (Hbhz), isonicotinoyl hydrazide (Hinh), nicotinoyl hydrazide (Hnah) and furoyl hydrazide (Hfah)} react with $[Mo^{VI}O_2(acac)_2]$ (Hacac = acetylacetone) in equimolar ratio in methanol to give dioxidomolybdenum(VI) complexes, $[MoO_2$(ap-bhz)(MeOH)] **1**, $[MoO_2$(ap-inh)(MeOH)] **2**, $[MoO_2$(ap-nah)(MeOH)] **3** and $[MoO_2$(ap-fah)(MeOH)] **4**. Reaction of these ligands with in-situ generated oxidoperoxidomolybdenum(VI) precursor results in the formation of oxidoperoxidomolybdenum(VI) complexes, $[MoO(O_2)$(ap-bhz)(MeOH)] **5**, $MoO(O_2)$(ap-inh)(MeOH)] **6**, $MoO(O_2)$(ap-nah)(MeOH)] **7** and $MoO(O_2)$(ap-fah)(MeOH)] **8**. These complexes have been characterized by elemental analysis, spectroscopic techniques (infrared, UV-vis, ^{1}H and ^{13}C NMR) and thermogravemetric analysis. Structures of complexes $[Mo^{VI}O_2$(ap-bhz)$(H_2O)]$ **1a** (water coordinated), $[Mo^{VI}O_2$(ap-bhz)(DMSO)] **1b** (DMSO coordinated), $[Mo^{VI}O_2$(ap-nah)(DMF)] **3a** (DMF coordinated), $[Mo^{VI}O(O_2)$(ap-bhz)(MeOH)] **5** (methanol coordinated) and $[Mo^{VI}O(O_2)$(Hap-nah)(OMe)]·MeOH **7a** (methoxy coordinated) have been confirmed by single crystal X-ray study. X-ray diffraction study also reveals that tridentate ligands bind to the metal center through enolic oxygen (of pyrazolol), azomethine nitrogen and enolic oxygen (of hydrazide) atoms. In complex **7a**, pyridinic nitrogen is protonated. These complexes [dioxidomolybdenum(VI) as well as oxidoperoxidomolybdenum(VI)] have been tested as catalysts for the temperature dependent one pot three components (methylacetoacetate, benzaldehyde and ammonium acetate) dynamic

covalent assembly, via Hantzsch reaction, using 30% H_2O_2 as an greener oxidant under solvent free condition. Various parameters such as amounts of catalyst, oxidant and temperature of the reaction mixture have been taken into consideration to optimize the reaction conditions. In Hantzsch reaction, temperature and oxidant control the conversion and selectivity of the desired product.

---

† Electronic supplementary information (ESI) available: TGA detail and X-ray crystal structure for complex 1a and figures related to π-π interaction in complexes, UV-vis spectra of ligands and complexes. CCDC 1436144-1436148 for complexes, **1a**, **1b**, **3a**, **5** and **7a**. For ESI and crystallographic data in CIF or other electronic format see
DOI: xxxxxxx

Introduction

Dihydropyridine (DHP) is an important class of organic moiety found in a large number of biologically active and potential therapeutic compounds.[1] The pharmacological activities of dihydropyridine containing compounds involve anticancer,[2] neurotropic,[3] glycoprotein inhibitors,[4] bronchodilating[5] and antidiabetic.[6] Synthesis of DHPs by one pot multi components dynamic covalent assembly [also called multicomponent reaction (MCR)] method, initially introduced by Arthur Hantzsch in 1882, is efficient, environmentally benign, less time consuming and cost effective.[7] This method offers a wide range of possibilities for the efficient construction of highly complex molecules. Efforts have been made to synthesize derivatives of DHPs by varying aldehyde, ammonia source and β-keto ester (or using β-diketones, malonic acid esters, β-keto acids, β-aminocrotononitrile, ethylcyanoacetate, cyanoacetamide etc. in place of β-keto esters).[8] The oxidation of DHPs to the corresponding pyridine derivatives is the prime metabolic route in biological systems.[9] Hantzsch pyridine, obtained through aromatization of the corresponding dihydropyridine shows interesting biological activity, which is attributed due to its resemblance with reduced form of nicotinamide adenine dinucleotide (NADH).[10] Various types of homogeneous and heterogeneous catalysts have also been used in synthesizing derivatives of DHP and pyridine.[1,8,11]

Molybdenum complexes are well known for their catalytic applications in the oxidation of organic substrates.[12-14] Hydrazones of 4-aryl-3-methyl-1-phenyl-5-pyrazolone have shown excellent coordinating potential towards molybdenum.[12] Catalytic oxidation of secondary

alcohols to the corresponding aldehydes by these complexes has been carried out in the presence and absence of N-based additive.[12] Herein, we have considered hydrazones of 4-acetyl-3-methyl-1-phenyl-5-pyrazolone (Scheme 1) having several electron-rich donor centers and have prepared dioxidomolybdenum(VI) and oxidoperoxidomolybdenum(VI) complexes. After complete characterization, these complexes have been tested as catalysts for the Hantzsch reaction under atmospheric conditions to obtain dimethyl-2,6-dimethyl-4-phenyl-1,4-dihydropyridine-3,5-dicarboxylate and related product(s) by the reaction of methylacetoacetate, benzaldehyde and ammonium acetate using greener oxidant H_2O_2 under solvent free condition.

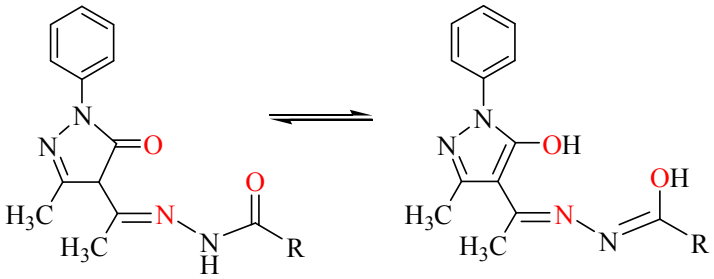

R	Ligands	R	Ligands
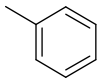	H_2ap-bhz **I**	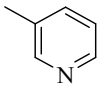	H_2ap-nah **III**
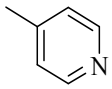	H_2ap-inh **II**		H_2ap-fah **IV**

Scheme 1 Hydrozones derived from 4-acetyl-3-methyl-1-phenyl-2-pyrazoline-5-one used in this study. Keto-enol tautomerism of a general structure of hydrazones is also shown here.

Experimental section

Materials

Ammonium molybdate tetrahydrate, isonicotinoylhydrazide (Hinh), nicotinoylhydrazide (Hnah) and methylacetoacetate (Loba Chemie, India), 2-furoylhydrazide (Hfah), acetylacetone (Hacac), phenylhydrazine (Aldrich, U.S.A.) were used as supplied. Ethylacetoacetate, diethylether, 30% aqueous H_2O_2, glacial acetic acid and benzaldehyde were procured from Renkem, India. Benzoyl

hyrazide (Hbhz) was prepared by the reaction of a twofold excess of hydrazine hydrate with ethylbenzoate. All other chemicals and solvents used were purchased from certified companies and used as supplied. $[Mo^{VI}O_2(acac)_2]$,[15] 3-methyl-1-phenyl-5-pyrazolone[16] and 4-acetyl-3-methyl-1-phenyl-2-pyrazoline-5-one[17] were synthesized following the literature-reported methods.

Instrumentation and Characterization Procedures

Elemental (C, H and N) analysis of ligands and complexes was obtained on Elementar analyser instrument model Vario-El-III. Thermogravimetric analysis (TGA) of the complexes was carried out using TG Stanton Redcroft STA 780. Infrared spectra were recorded as KBr pellets on a Nicolet 1100 FT-IR spectrometer after grinding the sample with KBr. UV-vis absorption spectra of ligands and complexes were recorded on a Shimadzu single beam spectrophotometer in methanol. ^{1}H and ^{13}C NMR spectra were obtained in DMSO-d_6 on a JEOL 400 MHz spectrometer. The residual DMSO-d_6 signal at δ = 2.50 ppm, was used for calibration of the chemical shift scale. The oxidation products were analyzed with a Shimadzu 2010 plus gas-chromatograph fitted with Rtx-1 capillary column (30 m × 0.25 mm × 0.25 μm) and a FID detector. Identity of the products was confirmed by Shimadzu QP-5000 GC-MS.

X-Ray single crystal diffraction studies

Three-dimensional X-ray data were collected on a Bruker Kappa Apex CCD diffractometer at room temperature for **1a** (Fig. S1), **1b** and **5**, and at low temperature (100 K) for **3a** and **7a**, by the ϕ-ω scan method. Reflections were measured from a hemisphere of data collected from frames, each of them covering 0.3º in ω. A total of 27898 for **1a**, 28606 for **1b**, 56274 for **3a**, 7803 for **5** and 45667 reflections for **7a** measured were corrected for Lorentz and polarization effects and for absorption by multi-scan methods based on symmetry-equivalent and repeated reflections. Of the total, 2236 for **1a**, 4067 for **1b**, 5857 for **3a**, 3635 for **5** and 3700 for **7a** independent reflections, respectively exceeded the significance level ($|F|/\sigma|F|$) > 4.0. After data collection, in each case an empirical absorption correction (SADABS)[18] was applied, and the structures were solved by direct methods and refined by full matrix least-squares on F^2 data using SHELX suite of programs.[19] In **1a** and **1b**, hydrogen atoms were included in calculated

position and refined in the riding mode, except the hydrogen atoms of water molecule O(5) in **1b**, which were located in difference Fourier map and left to refine freely. In **3a**, hydrogen atoms were located in difference Fourier map and left to refine freely, except for C(4), C(6), C(20) and C(21), which were included in calculated position and refined in the riding mode. In **5**, hydrogen atoms were located in difference Fourier map and left to refine freely, except for C(4), C(6) and C(20), which were included in calculated position and refined in the riding mode. In **7a**, hydrogen atoms were included in calculated position and refined in the riding mode, except the hydrogen atoms of C(9), C(11), C(12), C(14), C(15), C(16), C(17) and C(18). Refinements were done with allowance for thermal anisotropy of all non-hydrogen atoms. A final difference Fourier map showed no residual density outside: 0.408 and –0.422 e.Å^{-3} for **1a**, 0.332 and –0.485 for **1b**, 0.416 and –0.664 for **3a** and 0.502 and -0.689 for **5**. In **7a**, a final difference Fourier map showed high residual density outside due to a unrefined disorder on hydrogen atom of N(5), which is involved in hydrogen bond with O(6). A weighting scheme $w = 1/[\sigma^2(F_o^2) + (0.062600\ P)^2 + 3.353200\ P]$ for **1a**, $w = 1/[\sigma^2(F_o^2) + (0.027000\ P)^2 + 1.072800\ P]$ for **1b**, $w = 1/[\sigma^2(F_o^2) + (0.033900\ P)^2 + 0.604200\ P]$ for **3a**, $w = 1/[\sigma^2(F_o^2) + (0.040200\ P)^2 + 2.106900\ P]$ for **5** and $w = 1/[\sigma^2(F_o^2) + (0.058400\ P)^2 + 6.167200\ P]$ for **7a**, where $P = (|F_o|^2 + 2|F_c|^2)/3$, were used in the latter stages of refinement. Further details of the crystal structure determination are given in Table 1.

Table 1 Crystal data and structure refinement for $[Mo^{VI}O_2(ap\text{-}bhz)(H_2O)]$ **1b**, $[Mo^{VI}O_2(ap\text{-}nah)(DMF)]$ **3a**, $[Mo^{VI}O(O_2)(ap\text{-}bhz)(MeOH)]$ **5** and $[Mo^{VI}O(O_2)(Hap\text{-}nah)(OMe)]\cdot MeOH$ **7a**

	1b (CCDC 1436145)	**3a** (CCDC 1436146)	**5** (CCDC 1436147)	**7a** (CCDC 1436148)
Formula	$C_{19}H_{18}MoN_4O_5$	$C_{21}H_{22}MoN_6O_5$	$C_{20}H_{20}MoN_4O_6$	$C_{20}H_{23}MoN_5O_7$
Formula weight	478.31	534.39	508.34	541.37
T, *K*	296(2)	100(2)	293(2)	100(2)
Wavelength, Å	0.71073	0.71073	0.71073	0.71073
Crystal system	Monoclinic	Triclinic	Monoclinic	Monoclinic
Space group	$P2_1/n$	$P\bar{1}$	$P2_1/c$	$P2_1/c$
a/Å	9.4209(8)	7.7039(12)	7.6247(4)	7.4244(2)
b/Å	10.7591(10)	9.7133(15)	17.1429(9)	17.9776(6)
c/Å	19.0075(18)	15.248(2)	15.4107(10)	16.4764(5)
α/°	90	85.657(7)	90	90
β/°	93.017(5)	83.289(7)	94.512(3)	93.410(2)
γ/°	90	71.113(7)	90	90

V/Å^3	1923.9(3)	1071.3(3)	2008.1(2)	2195.26(12)
Z	4	2	4	4
F_{000}	968	544	1032	1104
D_{calc}/g cm^{-3}	1.651	1.657	1.681	1.638
μ/mm^{-1}	0.722	0.660	0.700	0.650
θ/ (°)	2.15 to 28.32	1.35 to 30.17	1.78 to 31.15	1.68 to 26.37
R_{int}	0.0320	0.0327	0.0240	0.0578
Crystal size/ mm^3	0.24 × 0.13 × 0.11	0.22 × 0.17 × 0.13	0.22 × 0.15 × 0.12	0.23 × 0.14 × 0.13
Goodness-of-fit on F^2	1.045	1.146	1.047	1.052
$R_1[I>2\sigma(I)]$ [a]	0.0245	0.0234	0.0396	0.0464
wR_2 (all data) [b]	0.0650	0.0705	0.1047	0.1226
Largest differences peak and hole (eÅ^{-3})	0.332 and -0.485	0.416 and -0.664	0.502 and -0.689	1.898 and -0.627

[a] $R_1 = \Sigma \| |F_o| - |F_c| \| / \Sigma |F_o|$. [b] $wR_2 = \{\Sigma[w(|F_o|^2 - |F_c|^2)^2] / \Sigma[w(F_o^2)^2]\}^{1/2}$

Synthetic procedures

H_2ap-bhz I. 4-Acetyl-3-methyl-1-phenyl-2-pyrazoline-5-one (1.08 g, 0.005 mol) and benzoylhydrazide (0.680 g, 0.005 mol) were dissolved separately in 15 mL of methanol in a reaction flask while heating in a water bath. Both solutions were mixed with shaking and the reaction mixture was refluxed in a water bath for 5 h. After cooling the reaction flask at room temperature for 12 h, the precipitated red solid was collected by filtration, washed with methanol and dried in a vacuum desiccator over silica gel. Yield: 1.43 g (85 %). (Found: C, 68.03; H, 5.22; N, 16.45 %. Calcd. for $C_{19}H_{18}N_4O_2$ (334.37): C, 68.25; H, 5.43; N, 16.76 %).

H_2ap-inh II. Ligand **II** was prepared from 4-acetyl-3-methyl-1-phenyl-2-pyrazoline-5-one (1.08 g, 0.005 mol) and isonicotinoylhydrazide (0.685 g, 0.005 mol) in methanol by the method used for **I**. The precipitated bright red solid was collected by filtration, washed with methanol and dried in a vacuum desiccator over silica gel. Yield: 1.51 g (89 %). (Found: C, 63.80; H, 4.99; N, 20.80 %. Calcd. for $C_{18}H_{17}N_5O_2$ (335.36): C, 64.47; H, 5.11; N, 20.88 %).

H_2ap-nah III. This ligand was prepared from 4-acetyl-3-methyl-1-phenyl-2-pyrazoline-5-one (1.08 g, 0.005 mol) and nicotinoylhydrazide (0.685 g, 0.005 mol) in methanol following the method used for **I**. The precipitated red solid was collected by filtration, washed with methanol and dried in a vacuum desiccator over silica gel. Yield: 1.40 g (83 %). (Found: C, 63.98; H, 5.01; N, 20.79 %. Calcd. for $C_{18}H_{17}N_5O_2$ (335.36): C, 64.47; H, 5.11; N, 20.88 %).

H_2ap-fah IV. Ligand **IV** was prepared following the method adopted for **I** from 4-acetyl-3-methyl-1-phenyl-2-pyrazoline-5-one (1.08 g, 0.005 mol) and 2-furoylhydrazide (0.63 g, 0.005 mol) in methanol. The precipitated light orange solid was collected by filtration, washed with methanol and dried in a vacuum desiccator over silica gel. Yield: 1.48 g (91 %). (Found: C, 62.33; H, 4.90; N, 17.21 %. Calcd. for $C_{17}H_{16}N_4O_3$ (324.33): C, 62.95; H, 4.97; N, 17.27 %).

[$Mo^{VI}O_2$(ap-bhz)(MeOH)] 1. Ligand **I** (1.67 g, 0.005 mol) was dissolved in 15 mL of methanol. A methanolic solution of [$Mo^{VI}O_2(acac)_2$] (1.63 g, 0.005 mol) was added to the above solution and the reaction mixture was refluxed for 4 h. The obtained colored solution was concentrated on a water bath to half of its volume and then cooled to room temperature. The separated orange solid was filtered, washed with cold methanol and dried in a vacuum desiccator over silica gel. Yield: 2.11 g (86 %). (Found: C, 48.64; H, 4.01; N, 11.30 %. Calcd. for $C_{20}H_{20}MoN_4O_5$ (492.34): C, 48.79; H, 4.09; N, 11.38 %). Slow crystallization from MeOH-H_2O (95 : 5) as well as DMSO-MeOH (90 : 10) gave suitable crystals {[$Mo^{VI}O_2$(ap-bhz)(H_2O)] **1a** and [$Mo^{VI}O_2$(ap-bhz)(DMSO)] **1b**} for X-ray analysis at room temperature.

[$Mo^{VI}O_2$(ap-inh)(MeOH)] 2. Complex **2** was prepared from [$Mo^{VI}O_2(acac)_2$] (1.63 g, 0.005 mol) and **II** (1.68 g, 0.005 mol) in methanol following the method described for **1.** The separated dark red solid was filtered, washed with cold methanol and dried in a vacuum desiccator over silica gel. Yield: 1.95 g (79 %). (Found: C, 45.86; H, 3.71; N, 14.08 %. Calcd. for $C_{19}H_{19}MoN_5O_5$ (493.32): C, 46.26; H, 3.88; N, 14.20 %).

[$Mo^{VI}O_2$(ap-nah)(MeOH)] 3. Complex **3** was prepared following the method adopted for **1** from [$Mo^{VI}O_2(acac)_2$] (1.63 g, 0.005 mol) and **III** (1.68 g, 0.005 mol) in methanol. The separated reddish orange solid was filtered, washed with cold methanol and dried in a vacuum desiccator over silica gel. Yield: 1.90 g (77 %). (Found: C, 45.91; H, 3.83; N, 14.05 %. Calcd. for $C_{19}H_{19}MoN_5O_5$ (493.32): C, 46.26; H, 3.88; N, 14.20 %). X-ray diffraction quality crystals for [$Mo^{VI}O_2$(bp-nah)(DMF)] (**3a**) were obtained from its DMF solution at room temperature.

[$Mo^{VI}O_2$(ap-fah)(MeOH)] 4. Complex **4** was prepared from [$Mo^{VI}O_2(acac)_2$] (1.63 g, 0.005 mol) and **IV** (1.62 g, 0.005 mol) in methanol following the method described for **1.** The separated red solid was filtered, washed with cold methanol and dried in a vacuum desiccator over silica gel. Yield: 2.01 g (83%). (Found: C, 44.69; H, 3.61; N, 11.49 %. Calcd. for $C_{18}H_{18}MoN_4O_6$ (482.30): C, 44.83; H, 3.76; N, 11.62 %).

[$Mo^{VI}O(O_2)$(ap-bhz)(MeOH)] 5. MoO_3 (0.720 g, 0.005 mol) was dissolved in aqueous 30% H_2O_2 (20 mL) and stirred at room temperature for 12 h. The obtained clear light yellow solution was filtered and was added drop wise to a filtered solution of **I** (1.67 g, 0.005 mol) dissolved in methanol (15 mL) with slow stirring. The stirring was continued for additional 14 h. During this period a pale orange solid precipitated out. This was filtered off, washed with methanol and dried in a vacuum desiccator over silica gel. Yield: 2.09 g (82 %). (Found: C, 46.90; H, 4.02; N, 10.81 %. Calcd. for $C_{20}H_{20}MoN_4O_6$ (508.34): C, 47.25; H, 3.97; N, 11.02 %). X-ray diffraction quality crystals for **5** were obtained from its methanolic solution at room temperature.

[$Mo^{VI}O(O_2)$(ap-inh)(MeOH)] 6. Complex **6** was prepared from MoO_3 (0.720 g, 0.005 mol) dissolved in aqueous 30% H_2O_2 (20 mL) and **II** (1.68 g, 0.005 mol) in methanol following the method described for **5.** The separated dull red solid was filtered, washed with cold methanol and dried in a vacuum desiccator over silica gel. Yield: 1.96 g (77 %). (Found: C, 44.79; H, 3.66; N, 13.63 %. Calcd. for $C_{19}H_{19}MoN_5O_6$ (509.32): C, 44.81; H, 3.76; N, 13.75 %).

[$Mo^{VI}O(O_2)$(ap-nah)(MeOH)] 7. Complex **7** was prepared similarly as described for **5** by the reaction of MoO_3 (0.720 g, 0.005 mol) dissolved in aqueous 30% H_2O_2 (20 mL) and **III** (1.68 g, 0.005 mol) in methanol. The separated orange solid was filtered, washed with cold methanol and dried in a vacuum desiccator over silica gel. Yield: 1.91 g (75 %). (Found: C, 44.54; H, 3.59; N, 13.58 %. Calcd. for $C_{19}H_{19}MoN_5O_6$ (509.32): C, 44.81; H, 3.76; N, 13.75 %). X-ray diffraction quality crystals for [$Mo^{VI}O(O_2)$(Hap-nah)(OMe)]·MeOH (**7a**) were obtained from its methanolic solution at room temperature.

[$Mo^{VI}O(O_2)$(ap-fah)(MeOH] 8. Similar to **5**, reaction of MoO_3 (0.720 g, 0.005 mol) dissolved in aqueous 30% H_2O_2 (20 mL) and H_2ap-fah (**IV**) (1.62 g, 0.005 mol) in methanol gave dark

orange solid, which filtered, washed with cold methanol and dried in a vacuum desiccator over silica gel. Yield: 2.00 g (80 %). Found: C, 43.34; H, 3.55; N, 11.11 %. Calcd. for $C_{18}H_{18}MoN_4O_7$ (498.30): C, 43.39; H, 3.64; N, 11.24 %).

Catalytic activity study-Hantzsch reaction with aqueous H_2O_2

Hantzsch reaction was carried out in a 50 mL round-bottom flask equipped with a reflux condenser. Under typical conditions, benzaldehyde (0.53 g, 0.005 mol), methylacetoacetate (1.16 g, 0.010 mol), ammonium acetate (0.462 g, 0.006 mol), catalyst (0.003 g) and oxidant aqueous 30% H_2O_2 (1.13 g, 0.010 mol) under solvent free condition were mixed and the obtained solution was magnetically stirred at desired temperature (i.e. 20, 40, 60 or 80 ^oC) using an oil bath. The reaction was monitored by withdrawing small aliquots of the reaction mixture at definite time interval, extracting with n-heptane and analyzing quantitatively by gas chromatograph. The identity of products was confirmed by GC–MS.

Results and discussion

Synthesis and characterization of complexes

The reaction between equimolar amounts of $[Mo^{VI}O_2(acac)_2]$ and hydrazones of 4-acetyl-3-methyl-1-phenyl-5-pyrazolone, **I** – **IV** (*cf*. Scheme 1) in refluxing methanol leads to the formation of dioxidomolybdenum(VI) complexes, $[Mo^{VI}O_2(ap\text{-}bhz)(MeOH)]$ **1**, $[Mo^{VI}O_2(ap\text{-}inh)(MeOH)]$ **2**, $[Mo^{VI}O_2(ap\text{-}nah)(MeOH)]$ **3** and $[Mo^{VI}O_2(ap\text{-}fah)(MeOH)]$ **4**, respectively [Eqn (1) considering **I** as representative example]. Dissolving MoO_3 in 30% H_2O_2 gave non-isolable oxidoperoxidomolybdenum(VI) species which upon reaction with ligands **I**, **II**, **III** or **IV** in methanol followed by recrystallization of isolated species from methanol gave the corresponding oxidoperoxidomolybdenum(VI) complexes, $[Mo^{VI}O(O_2)(ap\text{-}bhz)(MeOH)]$ **5**, $[Mo^{VI}O(O_2)(ap\text{-}inh)(MeOH)]$ **6**, $[Mo^{VI}O(O_2)(ap\text{-}nah)(MeOH)]$ **7**, $[Mo^{VI}O(O_2)(ap\text{-}fah)(MeOH)]$ **8**, respectively [Eqn (2) considering **I** as representative example].

$$[Mo^{VI}O_2(acac)_2] + H_2ap\text{-}bhz + MeOH \rightarrow [Mo^{VI}O_2(ap\text{-}bhz)(MeOH)] + 2Hacac \quad (1)$$

$$[Mo^{VI}O(O_2)_x(H_2O)_n]^{2+} + H_2ap\text{-}bhz + MeOH \rightarrow [Mo^{VI}O(O_2)(ap\text{-}bhz)(MeOH)] + nH_2O + x\text{-}1\ O_2 \quad (2)$$

All the complexes exist as monomer. Scheme 2 provides their possible structures which are based on the spectroscopic (IR, UV-vis, ^{1}H and ^{13}C NMR) data, elemental analysis and single crystal X-ray diffraction studies of $[Mo^{VI}O_2(ap\text{-}bhz)(H_2O)]$ **1a** $[Mo^{VI}O_2(ap\text{-}bhz)(DMSO)]$ **1b**, $[Mo^{VI}O_2(ap\text{-}nah)(DMF)]$ **3a**, $[Mo^{VI}O(O_2)(ap\text{-}bhz)(MeOH)]$ **5** and $[Mo^{VI}O(O_2)(Hap\text{-}nah)(OMe)]\cdot MeOH$ **7a**. These complexes are soluble in methanol, ethanol, acetonitrile, DMF and DMSO.

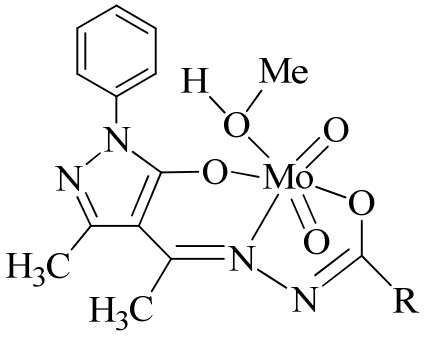

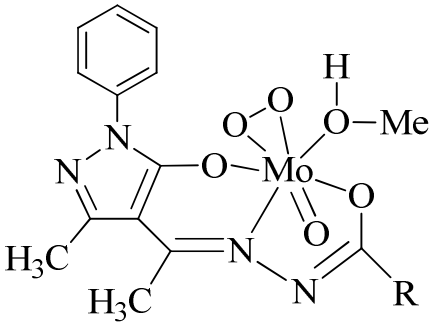

R	Complexes	R	Complexes
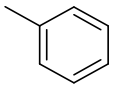	$[Mo^{VI}O_2(ap\text{-}bhz)(MeOH)]$ **1**	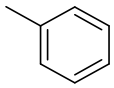	$[Mo^{VI}O(O_2)(ap\text{-}bhz)(MeOH)]$ **5**
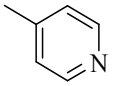	$[Mo^{VI}O_2(ap\text{-}inh)(MeOH)]$ **2**	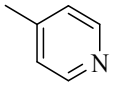	$[Mo^{VI}O(O_2)(ap\text{-}inh)(MeOH)]$ **6**
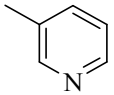	$[Mo^{VI}O_2(ap\text{-}nah)(MeOH)]$ **3**	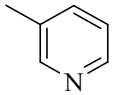	$[Mo^{VI}O(O_2)(ap\text{-}nah)(MeOH)]$ **7**
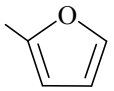	$[Mo^{VI}O_2(ap\text{-}fah)(MeOH)]$ **4**	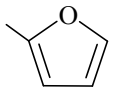	$[Mo^{VI}O(O_2)(ap\text{-}fah)(MeOH)]$ **8**

Scheme 2 Proposed structures of dioxido- and oxidoperoxidomolybdenum(VI) complexes.

Thermal Study

The thermal stability of the synthesized complexes has been studied under an oxygen atmosphere.[12] All complexes undergo mass loss roughly equal to one methanol molecule in the

temperature range 110–225 °C indicating the presence of coordinated methanol molecule. Upon further increasing the temperature, these complexes decompose exothermically in two/ three overlapping steps and form MoO_3 at ca. 540 °C.[12b,17] Table S1 presents details of the decomposition temperature range for the mass loss of methanol and the formation of MoO_3 along with their theoretical values for all complexes.

Structure description

ORTEP diagram for the compounds $[Mo^{VI}O_2(ap\text{-}bhz)(H_2O)]$ **1b**, $[Mo^{VI}O_2(ap\text{-}nah)(DMF)]$ **3a** $[Mo^{VI}O(O_2)(ap\text{-}bhz)(MeOH)]$ **5** and $[Mo^{VI}O(O_2)(Hap\text{-}nah)(OMe)]\cdot MeOH$ **7a** are shown in Figs. 1, 2, 3 and 4, respectively; ORTEP diagram for $[Mo^{VI}O_2(ap\text{-}bhz)(DMSO)]$ (**1a**) being kept in Fig. S1. Figs. S2-S6 show the π-π stacking interaction present in the crystal packing of these compounds. Selected bond distances and angles are given in Table 2.

The structures of the complexes **1a** (Fig. S1), **1b** and **3a** adopt a distorted six-coordinated octahedral geometry with the (ap-bhz) for **1a** and **1b** and (ap-nah) for **3a** as ligands, which act as tridentate, coordinating through the one $O_{pyrazoline\text{-}5\text{-}one}$, one $N_{hydrazide}$ and $O_{benzoyl}$ atoms. Mo centre completes the coordination sphere by bonding to two O_{oxido} terminal oxygen atoms and one oxygen atom of DMSO molecule in **1a** (Fig. S1), one oxygen atom of water molecule in **1b** and one oxygen atom of DMF molecule in **3a**. The axial sites are occupied by the oxido group O(2) and by the oxygen atoms [O(5)] of DMSO, H_2O and DMF molecules, respectively. The equatorial plane is formed by three atoms of the ligand and one of the terminal oxygen atoms, O(1), and it is slightly distorted with respect to the planarity, [mean deviation from the plane for O(1), N(3), O(3) and O(4): 0,0037(21) Å in **1a**, 0.0041(8) Å in **1b** and 0.0084(7) Å in **3a**]. The Mo-O_{oxido} bond lengths [Mo(1)-O(1) and Mo(1)-O(2) (see Table 2)] and bond angles [O=Mo=O angle are: 105.3(2)º in **1a**, 105.56(8)º in **1b** and 105.51(6)º in **3a**] are within the ranges for the bond distances typically observed in these type of compounds.[20]

The structures of the complexes **5** and **7a** adopt a distorted seven-coordinated pentagonal bipyramidal geometry with the (ap-bhz) for **5** and (Hap-nah) for **7a** as ligands, which act as tridentate, coordinating through the one $O_{pyrazoline\text{-}5\text{-}one}$, one $N_{hydrazide}$ and $O_{benzoyl}$ atoms, and Mo centre completes the coordination sphere bonding to one O_{oxido} terminal, one $O_{methanol}$ in **5** and one $O_{methoxo}$ in **7a**, and to two $O_{peroxido}$ atoms, O(2) and O(3), oxygen atoms. The axial sites are occupied by the oxido group, O(1), and the oxygen atom of methanol (in **5**) or methoxo (in **7a**)

groups, O(6). Hydrogen atom of methanol is close to pyridinic nitrogen making it protonated and leaving coordinated methanol as methoxy group (see Table 3). The equatorial plane is slightly distorted respect to the planarity, [mean deviation from plane for N(3), O(2), O(3), O(4), O(5): 0.0599(19) Å in **5** and 0.0101(22) Å in **7a**]. The Mo-O_{oxido}, Mo-$O_{peroxido}$ and O-O bond lengths (see Table 2) are within the ranges for the bond distances typically observed in these type of compounds.[21] The angles between the oxido ligand and the oxygen atoms of the peroxido group from 104.06(14)º and 103.36(15)º in **5**, and 102.42(16)º and 103.31(17)º in **7a**, also falling within the typically observed range (97-108º). The distance of peroxido bond O(2)-O(3) are 1.339(4) Å in **5** and 1.387(5) Å in **7a**, which are shorter than the usual range (ca. 1.41-1.51 Å).[21] Other bond lengths and angles are similar to those in other published complexes. [21]

In the crystal packing of compound **1a** (Fig. S2), two complexes of [$Mo^{VI}O_2$(ap-bhz)(DMSO)] interacting in an antiparallel placement, by π-π stacking between C=C bonds of pyrazoline group and centroids in phenyl groups.[22] The distances between centroids are in all cases: d_{c1-c2} = 3.541 Å {c1 [C(2I)-C(3I)], c2 [C(14C)-C(15C)-C(16C)-C(17C)-C(18C)-C(19C)]}. Instead of this in the compound **1b** the interaction is through benzoyl group and C=C bonds of pyrazoline group in a parallel position (see Fig. S3). The distances between centroids are in all cases: d_{c3-c4} = 3.858 Å {c3 [C(2A)-C(3A)], c4 [C(8D)-C(9D)-C(10D)-C(11D)-C(12D)-C(13D)]}. In the crystal packing of compound **3a**, pyridine and phenyl groups interacting by π-π stacking. The distances between centroids are in all cases: d_{c5-c6} = 3.683 Å {c5 [C(13K)-C(14K)-C(15K)-C(16K)-C(17K)-C18K)], c6 [C(8H)-C(9H)-C(10H)-C(11H)-C(12H)-N(5H)]} (see Fig. S4). In the crystal packing of compound **5**, the π-π stacking interaction is evaluated by fixing the distance between a centroid on benzoyl groups and atoms implied in double bonds like C(2K) and N(2L) of pyrazoline groups. The distances are: d_{C2K-C7}= 3.665 Å {c7 [C(8F)-C(9F)-C(10F)-C(11F)-C(12F)-C(13F)]} and d_{N2L-C5} = 3.671 Å (see Fig. S5). In the compound **7a**, stacking of several complexes are observed in the crystal packing. The distances between centroids are in all cases: d_{c8-c9} = 3.810 Å {c8 [C(13K)-C(14K)-C(15K)-C(16K)-C(17K)-C(18K), c9 [C(8G)-C(9G)-C(10G)-C(11G)-C(12G)-N(5G), the same for M and I complexes] and for M and G complexes: d_{c9-c10} = 3.739 Å {c10[C(8M)-C(9M)-C(10M)-C(11M)-C(12M)-N(5M)]} (see Fig. S6). Intermolecular hydrogen bonds are present in the crystal packing of the three compounds, **1b**, **5** and **7a** (see Table 3).

Table 2 Bond lengths and angles for the compounds $[Mo^{VI}O_2(ap\text{-}bhz)(H_2O)]$ **1b**, $[Mo^{VI}O_2(ap\text{-}nah)(DMF)]$ **3a,** $[Mo^{VI}O(O_2)(ap\text{-}bhz)(MeOH)]$ **5** and $[Mo^{VI}O(O_2)(Hap\text{-}nah)(OMe)]\cdot MeOH$ **7a**

Bond lengths	**1b**	**3a**	**5**	**7a**
Mo(1)-O(1)	1.6901(14)	1.7028(12)	1.673(3)	1.673(3)
Mo(1)-O(2)	1.6948(15)	1.6959(13)	1.892(3)	1.913(3)
Mo(1)-O(3)	1.9634(12)	1.9694(12)	1.887(3)	1.890(3)
Mo(1)-O(4)	1.9751(13)	1.9782(12)	1.994(2)	2.001(3)
Mo(1)-N(3)	2.2590(15)	2.2689(14)	2.212(3)	2.206(3)
Mo(1)-O(5)	2.3645(17)	2.2983(12)	2.002(2)	2.009(3)
Mo(1)-O(6)			2.340(3)	2.271(3)
N(1)-C(1)	1.351(2)	1.360(2)	1.357(4)	1.346(5)
N(1)-N(2)	1.383(2)	1.3869(19)	1.380(4)	1.389(5)
N(1)-C(14)	1.429(2)	N(1)-C(13) 1.424(2)	1.423(4)	N(1)-C(13) 1.424(2)
N(2)-C(3)	1.319(2)	1.317(2)	1.323(4)	1.318(5)
O(2)-O(3)			1.339(4)	1.387(5)
Angles	**1b**	**3a**	**5**	**7a**
O(1)-Mo(1)-O(2)	105.56(8)	105.51(6)	104.06(14)	102.42(16)
O(1)-Mo(1)-O(3)	100.36(6)	101.80(5)	103.36(15)	103.31(17)
O(2)-Mo(1)-O(3)	98.18(7)	98.26(6)	41.51(12)	42.77(15)
O(1)-Mo(1)-O(4)	97.10(7)	96.40(5)	96.50(13)	96.76(14)
O(2)-Mo(1)-O(4)	98.96(7)	96.92(6)	119.19(12)	120.80(14)
O(3)-Mo(1)-O(4)	151.21(6)	152.17(5)	78.36(12)	78.50(14)
O(1)-Mo(1)-N(3)	159.83(7)	159.79(6)	97.16(13)	92.02(14)
O(2)-Mo(1)-N(3)	93.37(7)	92.83(6)	153.34(12)	157.55(14)
O(3)-Mo(1)-N(3)	83.42(5)	83.49(5)	146.62(12)	149.48(14)
O(4)-Mo(1)-N(3)	72.65(6)	72.57(5)	73.33(9)	73.54(12)
O(1)-Mo(1)-O(5)	86.14(8)	85.18(5)	96.71(14)	97.35(14)
O(2)-Mo(1)-O(5)	168.30(7)	169.14(5)	78.06(12)	76.79(13)
O(3)-Mo(1)-O(5)	79.67(6)	81.06(5)	119.11(12)	118.76(14)
O(4)-Mo(1)-O(5)	78.86(6)	79.68(5)	154.68(10)	154.19(12)
N(3)-Mo(1)-O(5)	74.98(6)	76.32(5)	83.66(9)	84.45(11)
O(1)-Mo(1)-N(3)			97.16(13)	92.02(14)
O(3)-Mo(1)-N(3)			146.62(12)	149.48(14)
O(2)-Mo(1)-N(3)			153.34(12)	157.55(14)
O(4)-Mo(1)-N(3)			73.33(9)	73.54(12)
O(1)-Mo(1)-O(6)			172.79(12)	168.61(14)
O(3)-Mo(1)-O(6)			82.95(12)	88.05(16)
O(2)-Mo(1)-O(6)			82.95(12)	86.48(14)
O(4)-Mo(1)-O(6)			81.23(10)	84.49(12)
O(5)-Mo(1)-O(6)			82.97(10)	77.57(12)
N(3)-Mo(1)-O(6)			75.64(10)	77.43(12)

Table 3 Hydrogen bonds in the compounds $[Mo^{VI}O_2(ap\text{-}bhz)(H_2O)]$ **1b**, $[Mo^{VI}O(O_2)(ap\text{-}bhz)(MeOH)]$ **5** and $[Mo^{VI}O(O_2)(Hap\text{-}nah)(OMe)]\cdot MeOH$ **7a**

D-H...A (**compound**)	d(D-H)	d(H...A)	d(D...A)	<(DHA)
O(5)-H(5WB)...N(2)#1(**1b**)	0.78(3)	2.11(3)	2.884(2)	174(3)
O(5)-H(5WA)...O(2)#2(**1b**)	0.80(3)	2.07(3)	2.858(2)	174(3)
O(6)-H(6O)...N(2)#3 (**5**)	0.66(4)	2.17(4)	2.795(4)	158(5)
N(5)-H(5)...O(6)#4 (**7a**)	0.86	2.05	2.819(6)	149.0

Symmetry transformations used to generate equivalent atoms:

#1 -x+3/2,y+1/2,-z+1/2 #2 -x+1/2,y+1/2,-z+1/2 #3 x,-y+1/2,z-1/2 #4 x,-y+1/2,z-1/2

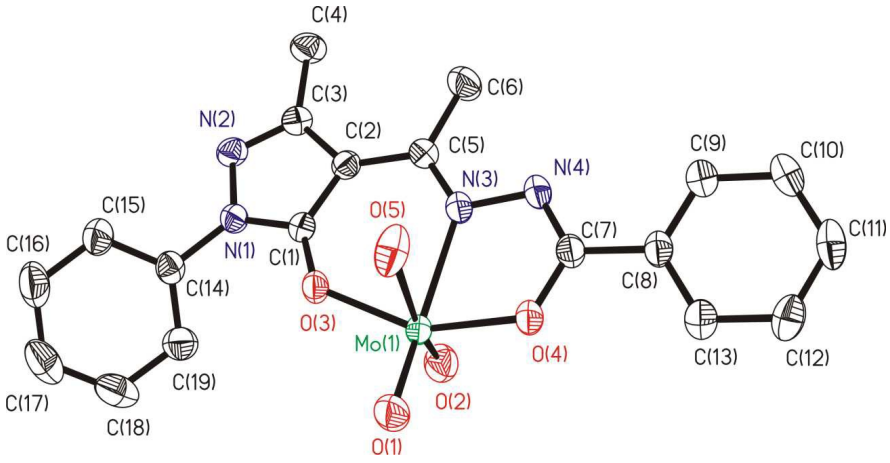

Fig. 1 ORTEP plot of complex $[Mo^{VI}O_2(ap\text{-}bhz)(H_2O)]$ **1b**. All the non-hydrogen atoms are presented by their 50% probability ellipsoids. Hydrogen atoms are omitted for clarity.

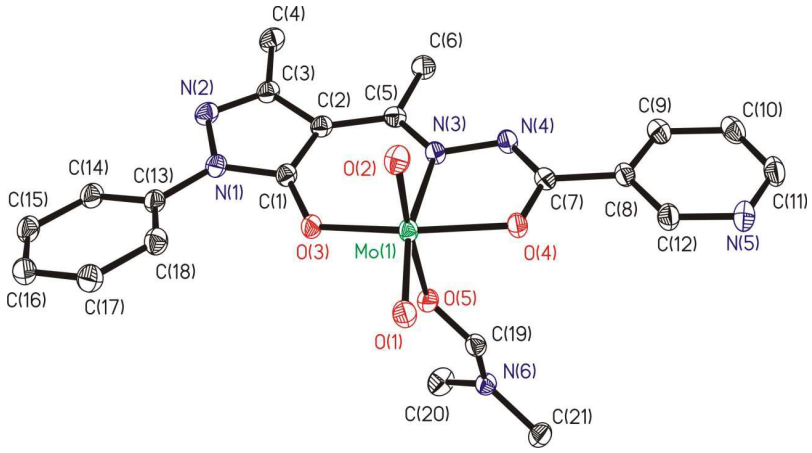

Fig. 2 ORTEP plot of complex in compound [$Mo^{VI}O_2$(ap-nah)(DMF)] **3a**. All the non-hydrogen atoms are presented by their 50% probability ellipsoids. Hydrogen atoms are omitted for clarity.

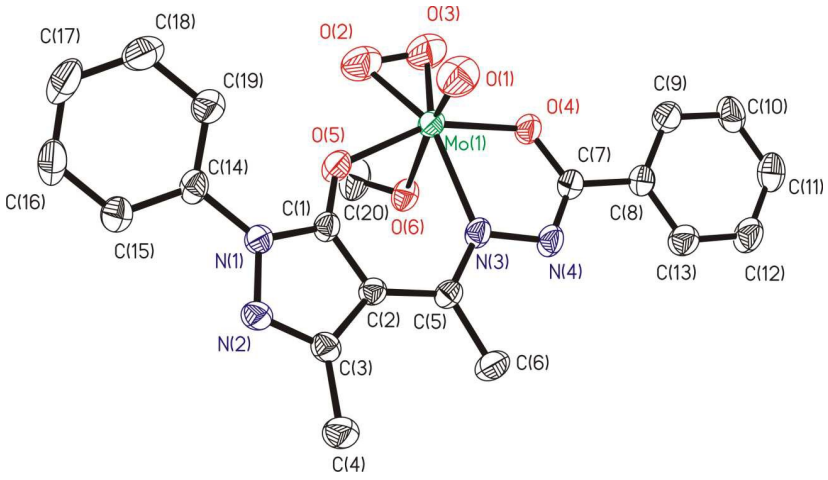

Fig. 3 ORTEP plot of complex [$Mo^{VI}O(O_2)$(ap-bhz)(MeOH)] **5**. All the non-hydrogen atoms are presented by their 50% probability ellipsoids. Hydrogen atoms are omitted for clarity.

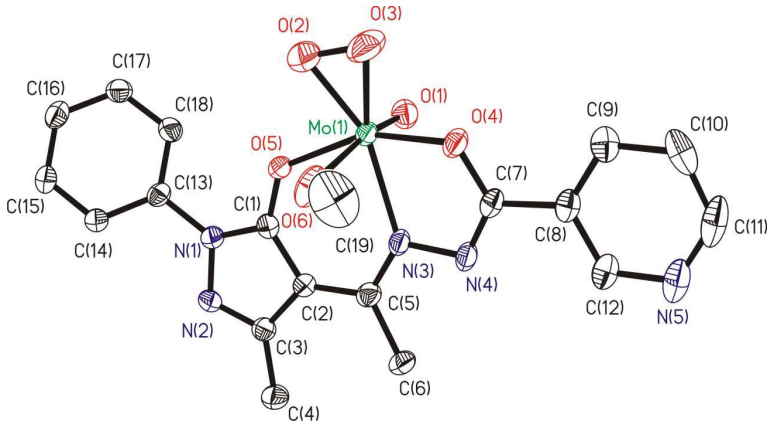

Fig. 4 ORTEP plot of complex in compound $[Mo^{VI}O(O_2)(Hap\text{-}nah)(OMe)]\cdot MeOH$ **7a**. All the non-hydrogen atoms are presented by their 50% probability ellipsoids. Hydrogen atoms are omitted for clarity.

IR spectroscopic study

Tables 4 and 5 present a partial list of IR spectral data of $[Mo^{VI}O_2]^{2+}$ and $[Mo^{VI}O(O_2)]^{2+}$ complexes, respectively along with the suitable assignment of the spectral bands.[17] The presence of $\upsilon(C{=}O_{hydrazide/pyrazolone})$ and υ(N-H) are indicative of the ketonic nature of ligands in the solid state. These bands disappear in complexes due to enolization of the ketonic group and replacement of H atom by the metal ion. A distinct band appearing in the region 1229-1261 cm^{-1} is assigned to the $\upsilon(C\text{-}O_{enolic})$ mode. A very sharp band appearing at 1514-1525 cm^{-1} in complexes compared to 1527-1539 cm^{-1} in ligands is indicative of the coordination of azomethine nitrogen atom. This coordination is explained as donation of the electron density from nitrogen to the empty d-orbital of the metal ion. A ligand band appearing at 1002-1017 cm^{-1} due to υ(N-N) is also affected upon coordination of nitrogen and appears at higher wave number by 8-22 cm^{-1} in complexes. The high frequency shift of the ν(N-N) band is expected because of reduced repulsion between the lone pairs of adjacent nitrogen atoms. The ligands exhibit a medium-intensity ν(OH) band covering the region 2925-2990 cm^{-1} due to intramolecular hydrogen bonds. In metal complexes this band is shifted to ca. 3430-3445 cm^{-1} indicating the breaking of this bond as well as plausible coordination of methanol.

The dioxidomolybdenum(VI) complexes are well characterized by two prominent peaks at 942-947 and 913-919 cm^{-1} which are assigned to $\upsilon_{asym}(O{=}Mo{=}O)$ and $\upsilon_{sym}(O{=}Mo{=}O)$

modes, respectively due to *cis*-[MoO_2] structure.[23] The oxidoperoxidomolybdenum(VI) complexes are distinguished by sharp peaks at 959-966 cm^{-1} due to υ(Mo=O), 829-856 cm^{-1} due to υ(O-O), 621-626 cm^{-1} due to $\upsilon_{asym}[Mo(O_2)]$ and 554-563 cm^{-1} due to $\upsilon_{sym}[Mo(O_2)]$ mode (Tables 4 and 5).[24]

Table 4 IR spectral data (cm^{-1}) of ligands and *cis*-$[Mo^{VI}O_2)]^{2+}$ complexes

Compound	υ(N-H)	υ (C=O) (hydrazide/pyrazolone)	υ(C=N)	$\upsilon(C\text{-}O_{enolic})$	υ(O=Mo=O)
H_2ap-bhz **I**	3175	1646 , 1590	1539		
$[Mo^{VI}O_2$(ap-bhz)(MeOH)] **1**			1515	1253	945 , 918
H_2ap-inh **II**	3140	1615 , 1586	1527		
$[Mo^{VI}O_2$(ap-inh)(MeOH)] **2**			1516	1250	943 , 918
H_2ap-nh **III**	3200	1626 , 1595	1538		
$[Mo^{VI}O_2$(ap-nah)(MeOH)] **3**			1514	1253	947 , 919
H_2ap-fah **IV**	3125	1630 , 1589	1537		
$[Mo^{VI}O_2$(ap-fah)(MeOH)] **4**			1515	1259	942 , 913

Table 5 IR spectral data (cm^{-1}) of $[MoO(O_2)]^{2+}$ complexes [a]

Complexes	υ(C=N)	$\upsilon(C\text{-}O_{enolic})$	υ(Mo=O)	υ(O-O)	$\upsilon\left(\begin{smallmatrix}O\\Mo\\O\end{smallmatrix}\right)^{b}$
$[Mo^{VI}O(O_2)$(ap-bhz)(MeOH)] **5**	1520	1261	962	833	621, 563
$[Mo^{VI}O(O_2)$(ap-inh) (MeOH)] **6**	1525	1245	965	837	621, 554
$[Mo^{VI}O(O_2)$(ap-nah) (MeOH)] **7**	1524	1248	966	856	624, 559
$[Mo^{VI}O(O_2)$(ap-fah) (MeOH)] **8**	1521	1229	959	829	626, 561

[a] For spectral data of the corresponding ligand see Table 4.

[b] asymmetric and symmetric bonds.

UV-vis spectral study

Uv-vis spectral data of ligands and their corresponding $[Mo^{VI}O_2]^{2+}$ and $[Mo^{VI}O(O_2)]^{2+}$ complexes are presented in Table 6 (Figs. S7, S8 and S9) present spectra of ligands and complexes). All four ligands exhibit very similar three characteristic absorption bands at 203-205, 248-251 and 347-385 nm due to transition between electronic energy levels, $\varphi \rightarrow \varphi^*$, $\pi \rightarrow \pi^*$

and n→π*, respectively.[25] As non-bonding electron pair are held more loosely than σ bonding electrons, these groups undergo transitions at higher wavelengths. In both types of molybdenum(VI) complexes, these bands generally shift towards lower wavelengths. In addition, a new band of medium intensity appears around 400 nm in $[MoO_2]^{2+}$ complexes and around 420 nm in $[MoO(O_2)]^{2+}$ complexes, which is assigned to a ligand to metal charge transfer (LMCT) band originating from electrons movement from filled p-orbital of ligand to the vacant d-orbital of metal ion of proper symmetry.[25] As Mo^{VI} -complexes have $4d^0$ configuration, d→d bands are not expected.

Table 6 UV-visible spectral data of ligands and dioxido- and oxidoperoxidomolybdenum(VI) complexes

Ligands and Complexes	λ_{max} / nm (ε/ $M^{-1}cm^{-1}$)
H_2ap-bhz **I**	347 (8.54×10^3), 281 (1.02×10^3), 248 (1.30×10^4), 227 (1.29×10^4), 205 (1.95×10^4)
H_2ap-inh **II**	385 (1.62×10^4), 283 (9.26×10^3), 250 (1.64×10^4), 203 (1.80×10^4)
H_2ap-nah **III**	375 (1.61×10^4), 279 (9.90×10^3), 249 (1.64×10^4), 201 (2.06×10^4)
H_2ap-fah **IV**	378 (8.76×10^3), 362 (9.26×10^3), 289 (1.11×10^4), 251 (1.61×10^4), 204 (1.43×10^4)
$[Mo^{VI}O_2$(ap-bhz)(MeOH)] **1**	407 (4.43×10^3), 339 (1.34×10^4), 295 (1.65×10^4), 251 (2.18×10^4), 226 (2.44×10^4), 206 (2.79×10^4)
$[Mo^{VI}O_2$(ap-inh)(MeOH)] **2**	401 (5.27×10^4), 313 (1.34×10^4), 227 (2.48×10^4), 207 (2.90×10^4)
$[Mo^{VI}O_2$(ap-nah)(MeOH)] **3**	404 (2.86×10^3), 307 (1.37×10^4), 240 (2.36×10^4), 212 (2.73×10^4)
$[Mo^{VI}O_2$(ap-fah)(MeOH)] **4**	413 (7.01×10^3), 341 (1.03×10^4), 295 (1.85×10^4), 253 (2.55×10^4), 209 (2.89×10^4)
$[Mo^{VI}O(O_2)$(ap-bhz)(MeOH)] **5**	423 (3.28×10^3), 325 (9.38×10^3), 238 (1.53×10^4), 201 (2.23×10^4)
$[Mo^{VI}O(O_2)$(ap-inh)(MeOH)] **6**	415 (5.43×10^3), 332 (1.36×10^4), 233 (2.12×10^4), 205 (2.49×10^4)
$[Mo^{VI}O(O_2)$(ap-nah)(MeOH)] **7**	413 (6.77×10^3), 323 (1.84×10^4), 240 (2.80×10^4), 206 (3.48×10^4)
$[Mo^{VI}O(O_2)$(ap-fah)(MeOH)] **8**	429 (4.69×10^4), 329 (1.83×10^4), 243 (2.21×10^4), 203 (2.71×10^4)

^{1}H and ^{13}C NMR studies

The coordinating modes of hydrazones, **I** – **IV** were confirmed by comparing their ^{1}H NMR spectral patterns with those of the corresponding complexes. The relevant spectral data are collected in Table 7 and representative spectra of a ligand and its complexes [i.e. H_2ap-bhz **I**, [$Mo^{VI}O_2$(ap-bhz)(MeOH)] **1** and [$Mo^{VI}O(O_2)$(ap-bhz)(MeOH)] **5**] is presented in Fig. 5. The ^{1}H NMR spectra of the ligands exhibit a signal at δ = 11.27 ppm (in **I**), δ = 11.47 ppm (in **II**), δ = 11.50 ppm (in **III**) and at δ = 11.32 ppm (in **IV**) due to –NH proton indicating their existence in their ketonic form. This is further supported by the appearance of a signal at δ = 2.33-2.35 ppm due to ring proton of pyrazole residue. Absence of these signals in $[Mo^{VI}O_2]^{2+}$ as well as $[Mo^{VI}O(O_2)]^{2+}$ complexes is in agreement with the enolization and subsequent replacement of H by the metal ion. Protons due to aliphatic groups (CH_3) exhibit prominent signals at δ = 2.40-2.46 and δ = 2.36-2.37 ppm. Signals due to these aliphatic protons appear at slightly down field (δ = 2.73-2.87 and δ = 2.46-2.51 ppm) in complexes. The methyl and alcoholic protons of the coordinated methanol in complexes appear at δ = 3.15-3.16 and 4.12-4.13 ppm, respectively. Thus, ^{1}H NMR data are consistent with the ONO dibasic tridentate binding mode of ligands and are in agreement with the conclusions drawn from IR data.

Table 7 ^{1}H NMR chemical shifts [δ in ppm] of ligands and complexes recorded in DMSO-d_6

Compounds [a]	-NH-	Pyrazolone (CH)	Aliphatic protons ($-CH_3$)	Aromatic protons
I	11.27 (s, 1H)	2.33 (s, 1H)	2.40 (s, 3H), 2.36 (s, 3H)	7.99-7.97 (d, 3H), 7.41-7.33 (m, 5H), 7.15-7.11 (t, 1H), 6.73-6.72 (q, 1H)
1			2.79 (s, 3H), 2.49 (s, 3H)	7.98-7.96 (d, 2H), 7.67-7.65 (d, 2H), 7.56-7.47 (m, 5H), 7.37-7.33 (t, 1H)
5			2.87 (s, 3H), 2.51 (s, 3H)	8.11-8.09 (d, 2H), 7.97-7.95 (d, 2H), 7.59-7.51 (m, 5H), 7.38-7.36 (d, 1H)
II	11.47 (s, 1H)	2.34 (s, 1H)	2.44 (s, 3H), 2.36 (s, 3H)	8.81 (s, 2H), 7.98-7.96 (d, 2H), 7.84-7.83 (d, 2H), 7.41-7.37 (t, 2H), 7.15-7.11 (t, 1H)
2			2.81 (s, 3H), 2.48 (s, 3H)	8.72 (s, 2H), 7.87-7.86 (d, 2H), 7.67-7.65 (d, 2H), 7.55-7.51 (t, 2H), 7.38-

				7.34 (t, 1H)
6			2.80 (s, 3H), 2.48 (s, 3H)	8.72 (s, 2H), 7.87-7.86 (d, 2H), 7.66-7.65 (d, 2H), 7.55-7.51 (t, 2H), 7.37-7.34 (t, 1H)
III	11.50 (s, 1H)	2.35 (s, 1H)	2.46 (s, 3H), 2.37 (s, 3H)	9.08 (s, 1H), 8.81-8.80 (d, 1H), 8.28-8.26 (d, 1H), 8.00-7.98 (d, 2H), 7.62-7.58 (q, 1H), 7.42-7.38 (t, 2H), 7.15-7.11 (t, 1H)
3			2.80 (s, 3H), 2.48 (s, 3H)	9.13 (s, 1H), 8.72 (s, 1H), 8.30-8.28 (d, 1H), 7.67-7.65 (d, 2H), 7.55-7.51 (t, 3H), 7.37-7.34 (t, 1H)
7			2.79 (s, 3H), 2.47 (s, 3H)	8.42-8.40 (d, 1H), 8.28-8.26 (d, 1H), 7.96-7.94 (d, 1H), 7.65-7.63 (d, 2H), 7.59-7.49 (m, 3H), 7.38-7.32 (q, 1H)
IV	11.32 (s, 1H)	2.34 (s, 1H)	2.45 (s, 3H), 2.37 (s, 3H)	7.94-7.92 (d, 2H), 7.64-7.63 (d, 1H), 7.58-7.54 (t, 2H), 7.42-7.38 (t, 2H), 7.15-7.11 (t, 1H)
4			2.73 (s, 3H), 2.47 (s, 3H)	7.91 (s, 1H), 7.66-7.64 (d, 2H), 7.54-7.50 (t, 2H), 7.37-7.33 (t, 1H), 7.12-7.11 (d, 1H), 6.68-6.67 (q, 1H)
8			2.73 (s, 3H), 2.46 (s, 3H)	7.97-7.95 (d, 2H), 7.66-7.64 (d, 1H), 7.59-7.49 (m, 2H), 7.38-7.32 (t, 1H), 7.11-7.10 (d, 1H), 6.72-6.66 (q, 1H)

[a] Letters given in parentheses indicate the signal structure: s = singlet, d = doublet, q = quartet, quin = quintet, m = multiplet.

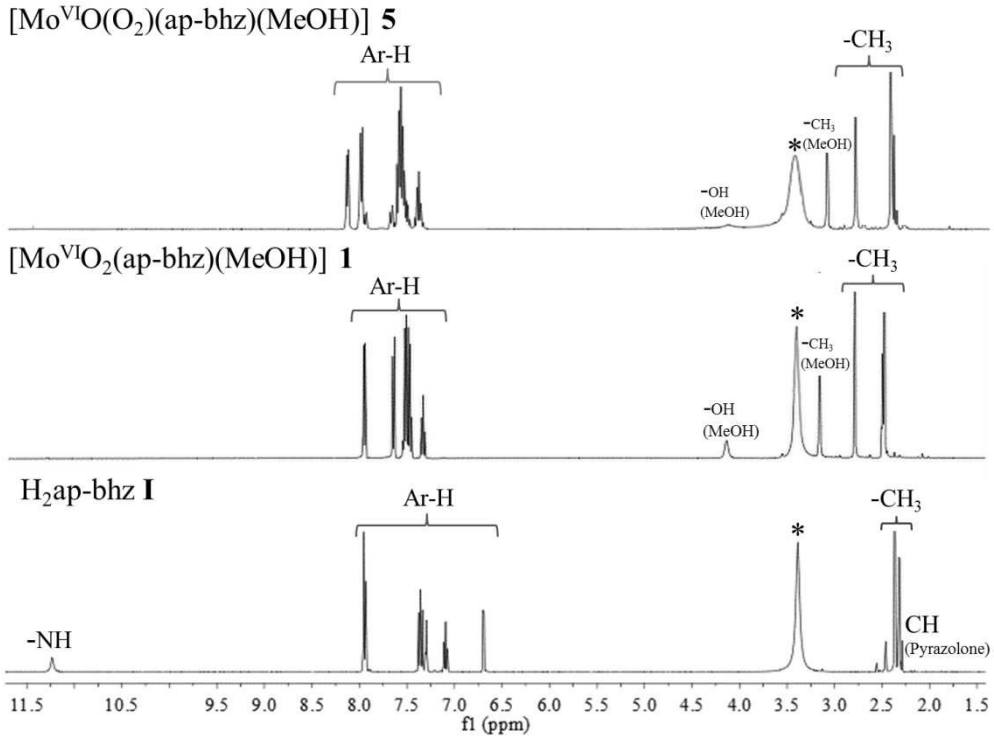

Fig. 5 ^{1}H NMR spectra of H_2ap-bhz **I**, [$Mo^{VI}O_2$(ap-bhz)(MeOH)] **1** and [$Mo^{VI}O(O_2)$(ap-bhz)(MeOH)] **5**.

Table 8 provides ^{13}C NMR spectral data of ligands and their corresponding $Mo^{VI}O_2$-complexes, and Fig. 6 provides representative spectra of a ligand and the corresponding $Mo^{VI}O_2$-complex. Comparison of the ^{13}C NMR spectra of ligands and corresponding complexes also provides useful information to confirm the structures of the complexes. Assignments of these signals are based on the intensity patterns of the chemical shifts of carbon atoms, the coordination-induced shifts [$\delta\Delta = \delta$(complex) – δ(free ligand)] of the signals for carbon atoms in the vicinity of the coordinating atoms[26] and Chemdarw® program. Ligands **I**, **II**, **III** and **IV** have 19, 18, 18 and 17 carbon atoms, respectively but only 15, 14, 15 and 15 ^{13}C NMR signals, respectively were observed for these ligands. Mostly same or more signals were present in the corresponding complexes. A large coordination induced shift of the signals for the carbon atoms associated with pyrazolol oxygen (C1), azomethine nitrogen (C4) and enolic oxygen (C13) (see Table 8) confirms the coordination of these functionalities to the molybdenum. The signals for carbon atoms (C2 and C3) closure to the above carbons were only slightly affected. The signal due to methyl carbon (C5 and C6) was observed at 17.02-17.19 and 16.76-16.82 ppm,

respectively, in all complexes while that of coordinated methanol (i.e. C14) was observed at ca. 53 ppm in all complexes.

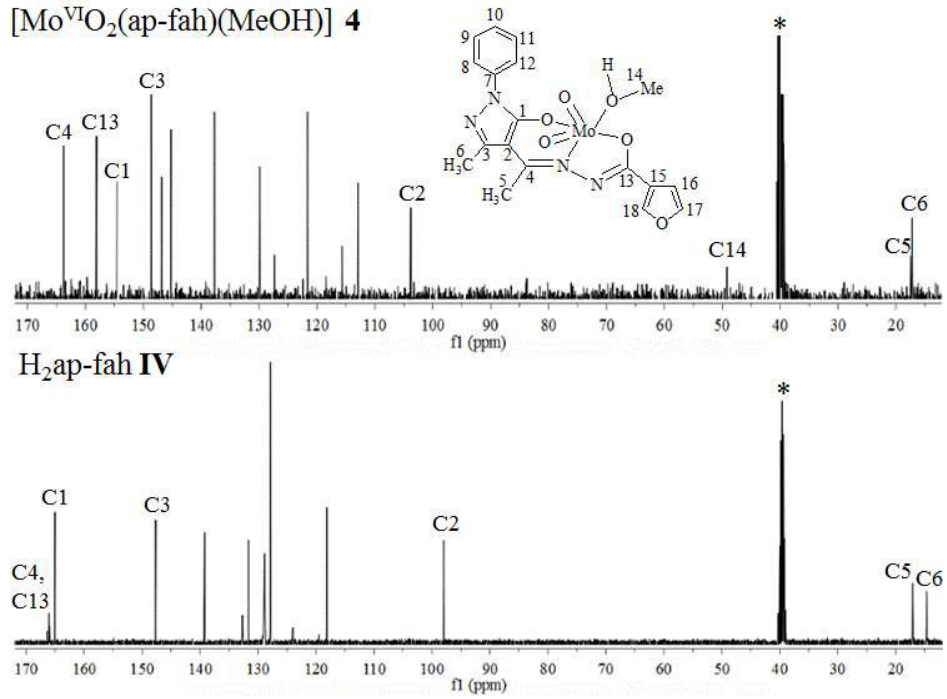

Fig. 6 ^{13}C NMR spectra of H_2ap-fah **IV** and [Mo$^{VI}O_2$(ap-fah)(MeOH)] **4**.

Table 8 ^{13}C NMR spectral data of ligands and complexes

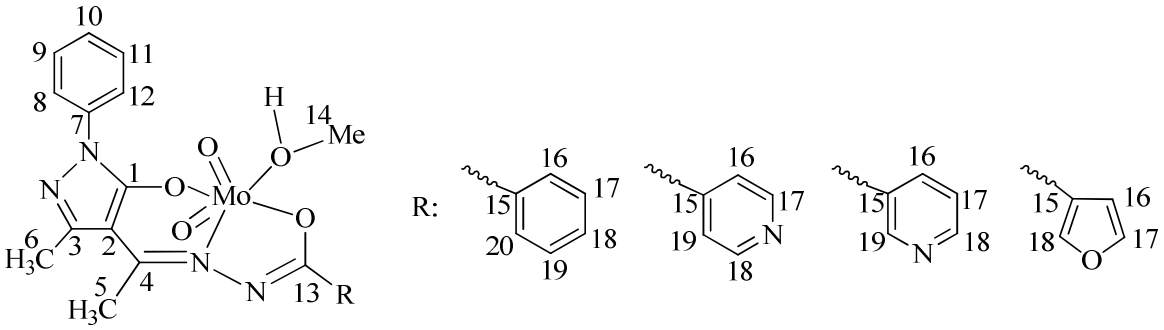

Compds.	C1	C2/ C3	C4	C5/ C6	C7	C8/C12; C9/C11	C10	C13	C14	R
I	157.04	98.03, 147.58	166.55	16.97, 14.58	139.05	118.06, 128.81	123.98	164.91		146.58, 145.28, 116.17, 112.37
1	154.19	103.33,148.19	164.47	17.04,	137.29	121.17,	126.86	163.56	48.55	131.50, 130.36,
Δδ	(-2.85)		(-2.08)	16.79		128.82		(-1.35)		129.41, 127.72
II	156.47	98.13, 147.76	165.83	16.98, 14.76	139.10	118.23, 128.82	123.97	164.97		150.48, 139.27, 121.78
2	154.30	103.39,148.48	164.12	17.12,	137.16	121.29,	126.88	162.73	48.03	150.56, 137.84,
Δδ	(-2.17)		(-1.71)	16.82		129.47		(-2.24)		121.19
III	156.51	97.96, 147.59	165.93	16.97, 14.60	139.06	118.02, 128.81	123.84	164.89		152.95, 148.68, 135.69, 127.62
3	154.21	103.33,148.33	164.27	17.19,	137.22	121.23,	126.82	162.84	48.21	151.84, 148.57,
Δδ	(-2.30)		(-1.66)	16.80		129.44		(-2.05)		135.25, 126.54, 123.99
IV	156.92	97.85, 147.55	165.99	16.97, 14.58	139.08	118.02, 128.77	123.97	165.88		132.57, 131.54, 127.78, 123.83
4	154.05	103.35,148.14	163.32	17.02,	137.24	121.17,	126.88	164.61	49.62	146.37, 144.74,
Δδ	(-2.87)		(-2.67)	16.76		129.41		(-1.27)		115.15, 112.43

Catalytic activity

Hantzsch reaction, a three components dynamic covalent assembly comprising of methylacetoacetate, benzaldehyde and ammonium acetate under solvent free condition in the presence of oxidant and catalyst has been reported to give four different products[1]; Scheme 3. Using $[MoO_2]^{2+}$ and $[MoO(O_2)]^{2+}$ complexes as catalysts result in the formation of only two products, dimethyl 2,6-dimethyl-4-phenyl-1,4-dihydropyridine-3,5-dicarboxylate (a) and dimethyl 2,6-dimethyl-4-phenylpyridine-3,5-dicarboxylate (b).

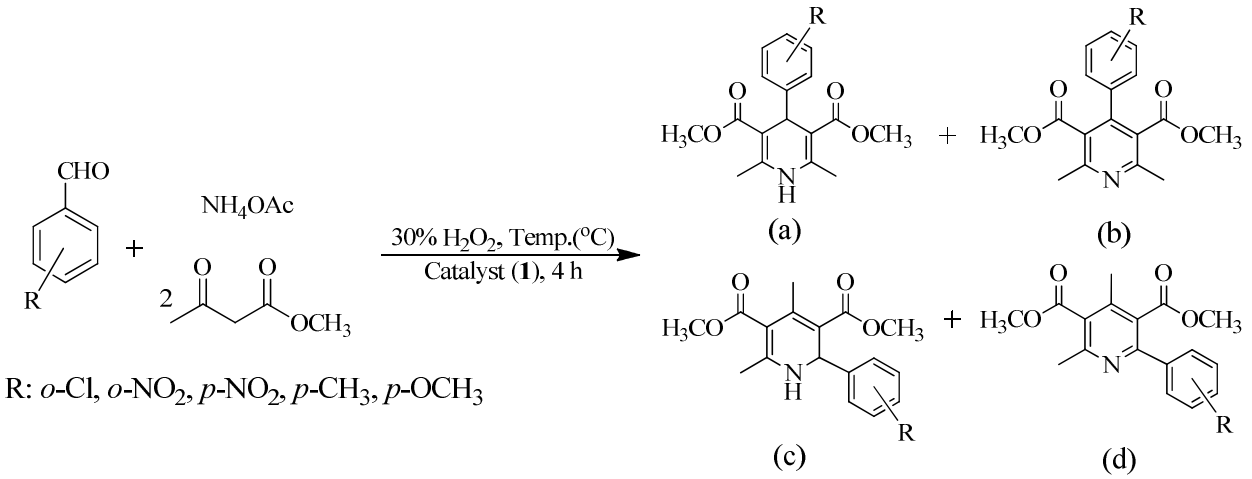

R: *o*-Cl, *o*-NO_2, *p*-NO_2, *p*-CH_3, *p*-OCH_3

Scheme 3 Four expected products of a Hantzsch reaction using reactants benzaldehyde, methylacetoacetate and ammonium acetate: (a) dimethyl 2,6-dimethyl-4-phenyl-1,4-hydropyridine-3,5-dicarboxylate and (b) dimethyl 2,6-dimethyl-4-phenylpyridine-3,5-dicarboxylate (c) dimethyl 2,4-dimethyl-6-phenyl-1,4-dihydropyridine-3,5-dicarboxylate (d) dimethyl 2,4-dimethyl-6-phenylpyridine-3,5-dicarboxylate

Here, we have studied the effect of temperature and amounts of catalyst and oxidant on the reactivity of these substrates and selectivity of products. Complex $[Mo^{VI}O_2(ap\text{-}bhz)(MeOH)]$ **1** was initially studied as a representative catalyst precursor. Thus, for 0.005 mol (0.53 g) of benzaldehyde, 0.010 mol (1.16 g) of methylacetoacetate, 0.006 mol (0.46 g) of ammonium acetate (1:2:1 molar ratio); three different amounts of catalyst precursor i.e. [2.03×10^{-6} mol (0.001 g), 4.06×10^{-6} mol (0.002 g) and 6.09×10^{-6} mol (0.003 g)] and aqueous 30% H_2O_2 (0.005, 0.010 and 0.015 mol) were taken in solvent free condition and the reaction was carried out at different temperatures (20, 40, 60, and 80 ^oC in particular). Table 9 summarizes all the conditions and the conversion of combined products (based on benzaldehyde taken) obtained under a particular set of conditions. Several conclusions can be drawn from these experiments:

(i) Independent of the amounts of catalyst and oxidant used, the conversion increases with time at a particular temperature of the reaction mixture and requires 4 h to attain the equilibrium. However, the most suitable temperature is 40 ^oC to carry out the reaction with highest conversion of the combined products after 4 h of reaction time.

(ii) Conversion of the combined products increases with the increment of amount of catalyst at a fixed amount of oxidant (Fig. 7).

(iii) Conversion of the combined products also increases with the increment of amount of oxidant at a fixed amount of catalyst. However, benzaldehyde to oxidant ratio of 1 : 2 for 0.005 mol of benzaldehyde is normally suitable amongst the three ratios (i.e. 1 : 1, 1 : 2 and 1 : 3) considered (Fig. 8).

(iv) Independent of the amounts of catalyst, oxidant and temperature of the reaction mixture, the selectivity of b is always higher than a, but the most suitable temperature to obtain highest selectivity (ca. 99%) of b is 60 ^{o}C.

Thus, reaction conditions mentioned in entry no. 10 of the Table 9 are the best one to get the good yield of the combined products with a maximum selectivity of product b at 40 ^{o}C in 4 h of reaction time. A maximum of 46 % yield of products was obtained when reaction was carried out with 5 mL of CH_3CN under the optimized reaction conditions with 1,4-dihydropyridine : 4-phenylpyridine selectivity of 11 : 89 using catalyst **1**. Blank reaction (i.e. without catalyst and benzaldehyde to oxidant ratio of 1: 2 at 0.005 mol of benzaldehyde) under similar reaction conditions, only 19 %, 27 %, 16 % and 22 % conversion of combined products in 4 h of reaction time was obtained at 20, 40, 60 and 80 ^{o}C, respectively. Conversion obtained in the absence of oxidant but in presence of catalyst **1** under atmospheric oxygen and solvent free conditions was 39 % at 40 ^{o}C.

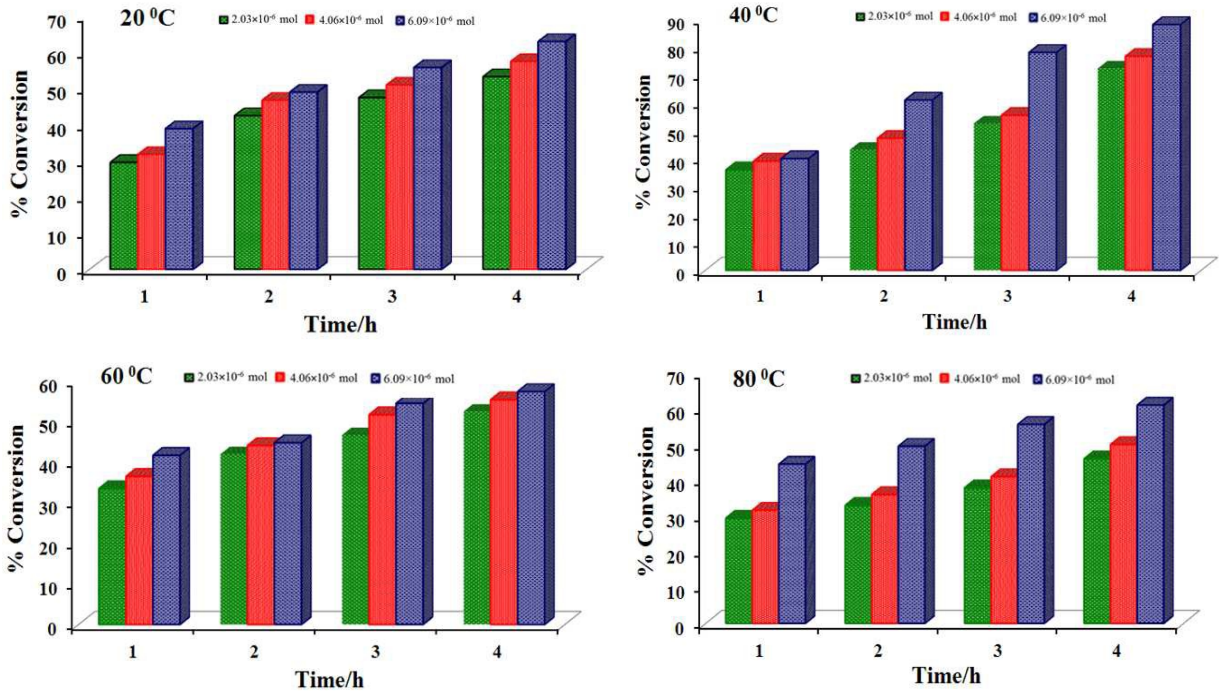

Fig. 7 Effect of amount of catalyst [$Mo^{VI}O_2$(ap-bhz)(MeOH)] **1** on the Hantzsch reaction. Reaction conditions: benzaldehyde (0.53 g, 0.005 mol), methylacetoacetate (1.16 g, 0.010 mol), ammonium acetate (0.462 g, 0.006 mol) and 30% aqueous H_2O_2 (1.13 g, 0.010 mol), under solvent-free condition at 20, 40, 60 and 80 ^oC for 4 h. Conversion was estimated by GC analysis.

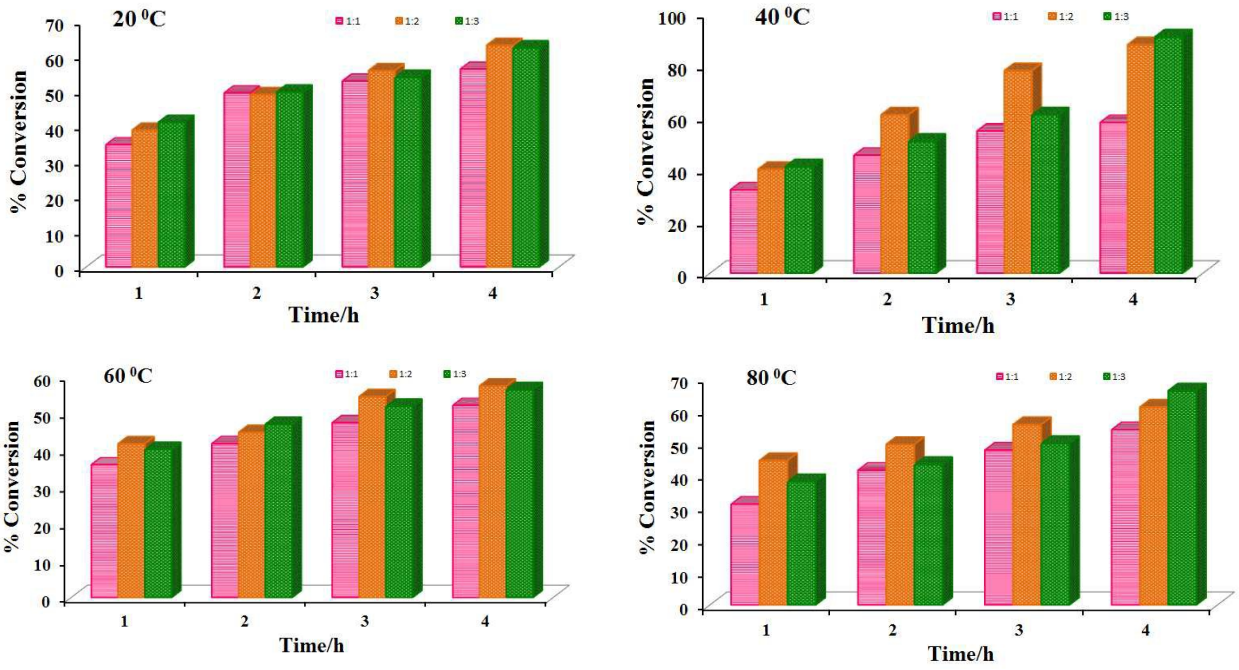

Fig. 8 Effect of amount of oxidant i.e. 30% H_2O_2 on the Hantzsch reaction. Reaction conditions: benzaldehyde (0.53 g, 0.005 mol), methylacetoacetate (1.16 g, 0.010 mol), ammonium acetate (0.462 g, 0.006 mol) and catalyst **1** [6.09×10^{-6} mol (0.003 g)], under solvent-free condition at 20, 40, 60 and 80 ^{0}C for 4 h.

Table 9 Conversion of 0.005 mol of benzaldehyde, 0.010 mol of methylacetoacetate, 0.006 mol of ammonium acetate into products using $[Mo^{VI}O_2(ap\text{-}bhz)(MeOH)]$ **1** as catalyst precursor in 4 h of reaction time under different reaction conditions.

Entry No.	Catalyst amount (g, mol)	Oxidant amount g (mol)	Temperature (^{0}C)	% Conversion	% Selectivity a	b
1.	0.001, 2.03×10^{-6}	1.13 (0.010)	20	53	4	96
2.	0.001, 2.03×10^{-6}	1.13 (0.010)	40	72	5	95
3.	0.001, 2.03×10^{-6}	1.13 (0.010)	60	52	1	99
4.	0.001, 2.03×10^{-6}	1.13 (0.010)	80	46	11	89
5.	0.002, 4.06×10^{-6}	1.13 (0.010)	20	58	19	81
6.	0.002, 4.06×10^{-6}	1.13 (0.010)	40	77	8	92
7.	0.002, 4.06×10^{-6}	1.13 (0.010)	60	55	1	99
8.	0.002, 4.06×10^{-6}	1.13 (0.010)	80	50	6	94
9.	0.003, 6.09×10^{-6}	1.13 (0.010)	20	63	21	79
10.[a]	**0.003**, 6.09×10^{-6}	**1.13 (0.010)**	**40**	**88**	**12**	**88**
11.	0.003, 6.09×10^{-6}	1.13 (0.010)	60	57	1	99
12.	0.003, 6.09×10^{-6}	1.13 (0.010)	80	61	9	91
13.	0.003, 6.09×10^{-6}	0.56 (0.005)	20	56	13	87
14.	0.003, 6.09×10^{-6}	0.56 (0.005)	40	58	6	94
15.	0.003, 6.09×10^{-6}	0.56 (0.005)	60	51	2	98
16.	0.003, 6.09×10^{-6}	0.56 (0.005)	80	54	3	97
17.	0.003, 6.09×10^{-6}	1.69 (0.015)	20	62	18	82
18.	0.003, 6.09×10^{-6}	1.69 (0.015)	40	91	10	90
19.	0.003, 6.09×10^{-6}	1.69 (0.015)	60	56	1	99
20.	0.003, 6.09×10^{-6}	1.69 (0.015)	80	66	7	93

[a] indicates the best suited reaction conditions to obtained good yield of combined products.

Under above optimized reaction conditions (i.e. entry no. 10 of Table 9), catalytic potentials of other complexes have also been tested for the same three components dynamic covalent assembly at four different temperatures (i.e. 20, 40, 60 and 80 ^{o}C) and results are summarized in Table 10. As noted above, 40 ^{o}C has been the best reaction temperature again to give highest yield of combined reaction products with ca. 90% selectivity of product b. Further, ca. 99% selectivity of b was noted when reaction was carried out at 60 ^{o}C. The peroxido group has not much effect on the catalytic activity as $MoO(O_2)$-complexes gave very similar results as obtained with the corresponding MoO_2-complexes.

Table 10 Percentage conversion and selectivity of Hantzsch reaction; employing catalyst **1** (6.09×10^{-6} mol), **2** (6.08×10^{-6} mol), **3** (6.08×10^{-6} mol), **4** (6.22×10^{-6} mol), **5** (5.90×10^{-6} mol), **6** (5.89×10^{-6} mol), **7** (5.89×10^{-6} mol) and **8** (6.02×10^{-6} mol) under optimized conditions at different temperatures in 4 h of reaction time

Temp. (^{0}C)	% Conversion (% Selectivity of a : b)[a]							
	1	**2**	**3**	**4**	**5**	**6**	**7**	**8**
20	63 (21 : 79)	59 (17 : 83)	61 (18 : 82)	56 (16 : 84)	70 (23 : 77)	61 (19 : 81)	60 (20 : 80)	63 (21 : 79)
40	88 (12 : 88)	67 (9 : 91)	63 (8 : 92)	62 (7 : 93)	83 (11 : 89)	71 (10 : 90)	65 (9 : 91)	66 (9 : 91)
60	57 (1 : 99)	55 (0 : 100)	58 (1 : 99)	49 (1 : 99)	60 (1 : 99)	57 (1 : 99)	59 (2 : 98)	54 (0 : 100)
80	61 (9 : 91)	53 (7 : 93)	59 (6 : 94)	51 (10 : 90)	66 (10 : 90)	69 (11 : 89)	65 (7 : 93)	62 (9 : 91)

[a] a: dimethyl 2,6-dimethyl-4-phenyl-1,4-dihydropyridine-3,5-dicarboxylate, b: dimethyl 2,6-dimethyl-4-phenylpyridine-3,5-dicarboxylate

In order to establish the scope of this novel reaction protocol and the selectivity ratio of different products at 40 and 60 ^{o}C under above optimized reaction conditions, we have also studied the effect of various substituents on benzaldehyde considering complex **1** as a catalyst precursor and results are summarized in Table 11. The electron withdrawing chloro- and nitro-groups (independent of the substitution position) on benzaldehyde show high conversion at both temperatures compared to electron donating methoxy and methyl substituents. However, within the two temperatures, as observed above, 40 ^{o}C is the suitable one to give better conversion in both cases.

Table 11 Effect of various substituents at benzaldehyde on the conversion and selectivity ratio of different products at 40 and 60 ^{o}C.

Substrates	% Conv [40 ^{o}C]	% Selectivity ratio [a : b]	% Conv [60 ^{o}C]	% Selectivity ratio [a : b]
2-Chlorobenzaldehyde	77	11 : 89	69	5 : 95
2-Nitrobenzaldehyde	69	15 : 85	50	1 : 99
4-Methylbenzaldehyde	59	7 : 93	43	3 : 97
4-Methoxybenzaldehyde	47	16 : 84	36	2 : 98
4-Nitrobenzaldehyde	63	14 : 86	41	2 : 98

Reactivity of $[Mo^{VI}O_2]^{2+}$ complexes with reactants of Hantzsch reaction and with H_2O_2 and possible reaction route of Hantzsch reaction

To establish possible routes of Hantzsch reaction, we have carried out interaction of reactants of Hantzsch reaction with complex **3** in MeOH. Thus, initially 10 mL of 2.1×10^{-4} M solution of **3** was treated with one drop portions of benzaldehyde solution (9.1×10^{-2} M) and the resultant spectroscopic changes are presented in Fig. 9 [**i** (b-d)]. The slow disappearance of LMCT band at 404 nm and simultaneously appearance of a new band at 283 nm suggests the interaction of benzaldehyde with complex **3**. Upon addition of one drop portions of β-ketoester solution to the above solution, the band at 283 nm slowly disappears and the LMCT band at 404 nm again becomes prominent to some extent [**i** (e-h) of Fig. 9]. Other two bands appearing at 330 and 380 nm in **3** remain at same positions with slight increase in intensity. Drop wise addition of β-ketoester solution (6.3×10^{-2} M) to 10 mL complex **3** solution (2.1×10^{-4} M) in methanol results in the generation of no new band except slight increase of intensity of existing bands **[ii** (b-e) of Fig. 9], indicating that there is possibly weak interaction of acidic hydrogen atom of β-ketoester with lone pair of electrons present on nitrogen atoms of the ligand system of complex **3**. However, addition of benzaldehyde solution to the above reaction mixture, a new band starts to appear at 283 nm which gains intensity upon further addition of benzaldehyde [**ii** (f-k) of Fig. 9]. All these observations possibly suggest the interaction of $[Mo^{VI}O_2]^{2+}$ complex with benzaldehye followed by its reaction with activated β-ketoester to give Knoevenagel condensation product as an intermediate **I** (See Scheme 4).[1] This is further supplemented by reacting benzaldehyde (0.005 mol) and methylacetoacetate (0.005 mol) in the presence of H_2O_2 (0.010 mol) and catalyst **3** (6.09×10^{-6} mol) at 40 ^{o}C and analyzing the obtained reaction mixture for intermediate **I** [See Fig. S10 (a) and (b)]. Here 38% formation of the intermediate **I** was obtained in 4 h of reaction time. In the absence of catalyst only 8% reaction product was obtained. In the next step, second non-catalytic key intermediate **II** (See Fig. S11) forms by the interaction of second molecule of β-ketoester with ammonium acetate.[10b-d] Non-catalytic interaction of intermediates **I** and **II** (i.e. Step-3) to give dihydropyridine[10b-d] and catalytic conversion of dihydropyridine into corresponding pyridine (i.e. Step-4) are known in the literature.[10b,10e-g]

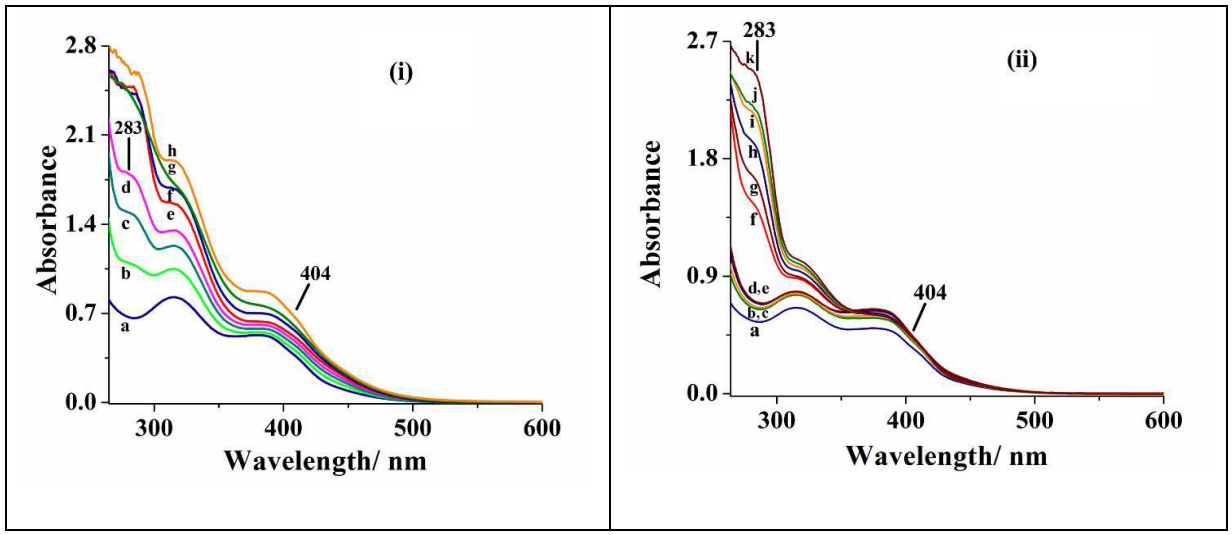

Fig. 9 Spectra **b-d** of (**i**): Spectral changes observed after successive addition of one drop portion of benzaldehyde (0.096 g, 0.91 mmol) dissolved in 10 mL of MeOH (final concentration of benzaldehyde solution; 9.1×10^{-2} M) to 10 mL of (2.1×10^{-4} M) solution of [$Mo^{VI}O_2$(ap-nah)(MeOH)] **3**. Spectra **e-h** of (**i**): Spectral changes observed after successive addition of one drop portion of methylacetoacetate (0.074 g, 0.64 mmol) dissolved in 10 mL of MeOH (final concentration of methylacetoacetate solution; 6.3×10^{-2} M). Spectra **b-e** of (**ii**): Spectral changes observed after successive addition of one drop portion of methylacetoacetate (0.074 g, 0.64 mmol) dissolved in 10 mL of MeOH (final concentration of methylacetoacetate solution; 6.3×10^{-2} M). Spectra **f-k** of (**ii**): Spectral changes observed after successive addition of one drop portion of benzaldehyde (0.096 g, 0.91 mmol) dissolved in 10 mL of MeOH (final concentration of benzaldehyde solution; 9.1×10^{-2} M) to 10 mL of (2.1×10^{-4} M) solution of **3**.

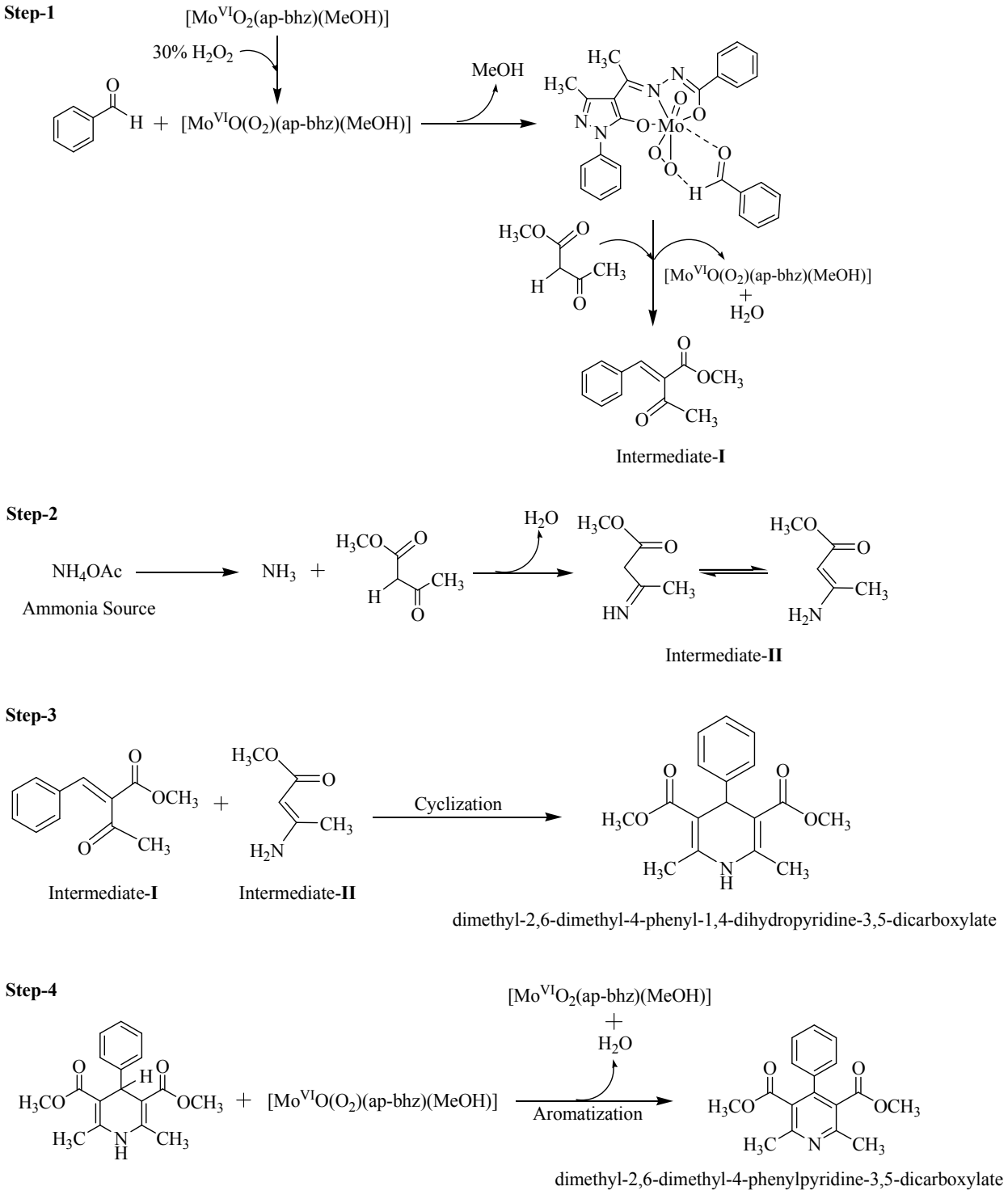

Scheme 4 Plausible mechanism for the formation of dimethyl 2,6-dimethyl-4-phenyl-1,4-dihydropyridine-3,5-dicarboxylate and the corresponding dimethyl 2,6-dimethyl-4-phenylpyridine-3,5-dicarboxylate.

As mentioned in the experimental section, $[Mo^{VI}O_2]^{2+}$ complexes react with H_2O_2 to give the corresponding $[Mo^{VI}O(O_2)]^{2+}$ complexes. The generation of such species has also been established in methanol by UV-visible spectroscopy. In a typical reaction, 20 mL of 5.6×10^{-5} M solution of $[Mo^{VI}O_2(ap\text{-}bhz)(MeOH)]$ **1** was treated with one drop portions of 30% aqueous H_2O_2 (0.066 g, 0.58 mmol) dissolved in 10 mL of methanol and the resultant spectroscopic changes are presented in Fig. 10. A considerable increase in the intensity of the 206 nm band and a broadening along with increase in intensity of 226 and 251 nm bands were observed [Fig. 10 (a)]. Another prominent band at 295 nm shows increase in intensity without any shift in position with successive addition of 30% aqueous H_2O_2. The band at 339 nm registers only slight change in intensity without any shift. All these changes suggest a minor structural change in the ligand environment upon interaction of H_2O_2 with complex. The LMCT band appearing at 402 nm (in higher concentration of methanolic solution) also shows its slight shifting to lower wavelength [Fig. 10 (b)] along with partial reduction in intensity possibly due to the formation of corresponding peroxido species.[12] Other $[Mo^{VI}O_2]^{2+}$ complexes have almost similar spectral changes except complex **2** where ligand bands show small but clear observable shifting; Fig. 10 [(c) and (d)]. However, the final spectra of all complexes are similar to the corresponding $[Mo^{VI}O(O_2)]^{2+}$ complexes. Thus, reaction of H_2O_2 with $[Mo^{VI}O_2]^{2+}$ complexes during catalytic reaction is likely to proceed through peroxido intermediate which helps in aromatization of dihydropyridine catalytically to facilitate the formation of the corresponding pyridine.

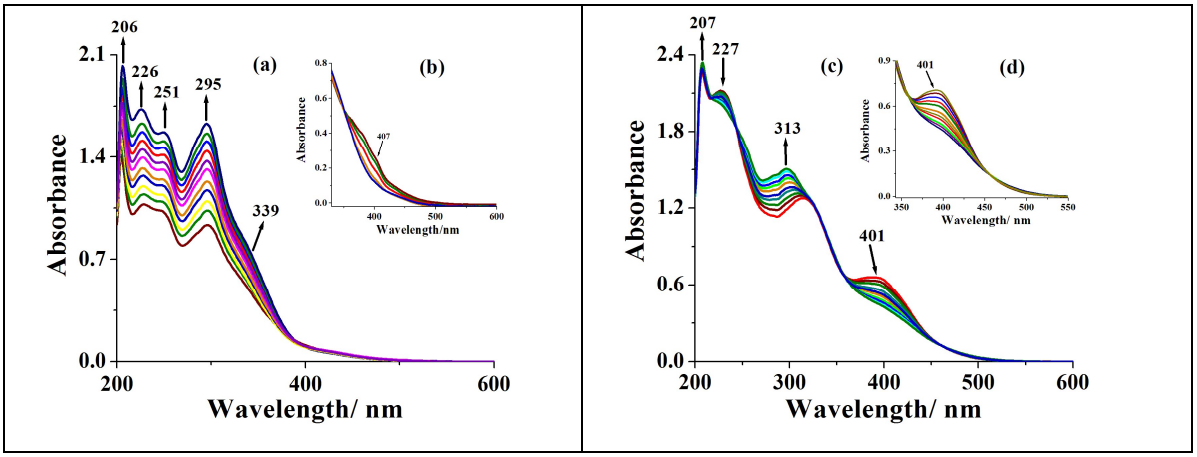

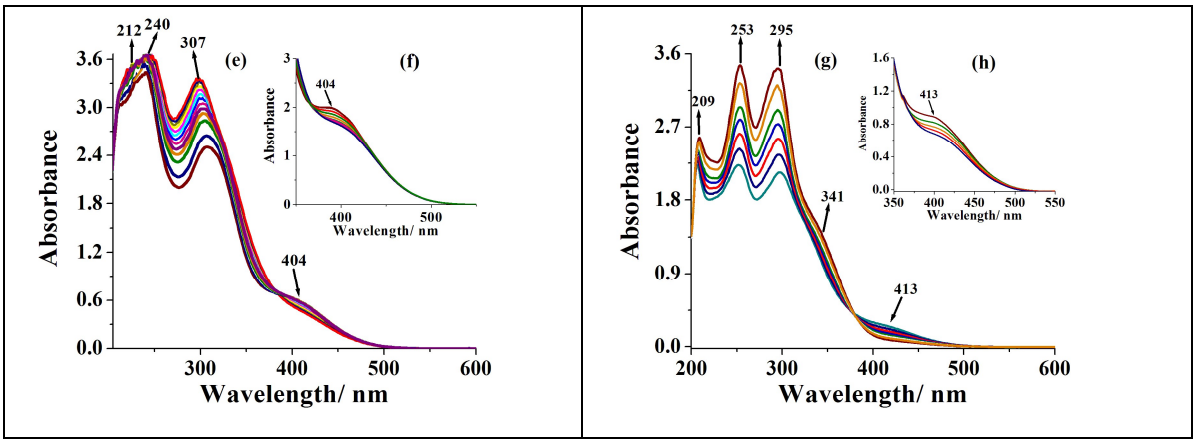

Fig. 10 (a) Spectral changes recorded after successive addition of one drop portion of 30% H_2O_2 (0.066 g, 0.58 mmol) dissolved in 10 mL of MeOH (final concentration of H_2O_2; 4.7×10^{-2} M) to 20 mL of (5.6×10^{-5} M) solution of [$Mo^{VI}O_2$(ap-bhz)(MeOH)] **1**. (b) Similar spectral changes with 30% H_2O_2 (0.061 g, 0.53 mmol) dissolved in 10 mL of methanol (final concentration of H_2O_2; 5.4×10^{-2} M) to 20 mL of methanolic solution (7.9×10^{-5} M) of complex **1**. (c) Spectral changes recorded after successive addition of one drop portion of 30% H_2O_2 (0.056 g, 0.49 mmol) dissolved in 10 mL of MeOH (final concentration of H_2O_2; 4.0×10^{-2} M) to 20 mL of 6.4×10^{-5} M solution of [$Mo^{VI}O_2$(ap-inh)(MeOH)] **2**. (d) Similar spectral changes with 30% H_2O_2 (0.059 g, 0.52 mmol) dissolved in 10 mL of methanol (final concentration of H_2O_2; 5.8×10^{-2} M) to 20 ml of methanolic solution (8.5×10^{-5} M) of compex **2**. (e) Spectral changes recorded after successive addition of one drop portion of 30% H_2O_2 (0.067 g, 0.59 mmol) dissolved in 10 mL of MeOH (final concentration of H_2O_2; 4.3×10^{-2} M) to 20 of mL of 7.2×10^{-5} M solution of [$Mo^{VI}O_2$(ap-nah)(MeOH)] **3**. (f) Similar spectral changes with 30% H_2O_2 (0.071 g, 0.63 mmol) dissolved in 10 mL of methanol (final concentration of H_2O_2; 6.1×10^{-2} M) to 20 ml of methanolic solution (7.8×10^{-5} M) of **3**. (g) Spectral changes recorded after successive addition of one drop portion of 30% H_2O_2 (0.063 g, 0.55 mmol) dissolved in 10 mL of MeOH (final concentration of H_2O_2; 5.2×10^{-2} M) to 20 mL of (7.5×10^{-5} M) solution of [$Mo^{VI}O_2$(ap-fah)(MeOH)] **4**. (h) Similar spectral changes with 30% H_2O_2 (0.074 g, 0.65 mmol) dissolved in 10 mL of methanol (final concentration of H_2O_2; 4.9×10^{-2} M) to 20 ml of methanolic solution (8.1×10^{-5} M) of **4**.

Conclusions

Dioxidomolybdenum(VI) complexes, [$Mo^{VI}O_2$(ap-bhz)(MeOH)] **1**, [$Mo^{VI}O_2$(ap-inh)(MeOH)] **2**, [$Mo^{VI}O_2$(ap-nah)(MeOH)] **3** and [$Mo^{VI}O_2$(ap-fah)(MeOH)] **4**, and their corresponding oxidoperoxidomolybdenum(VI) complexes, [$Mo^{VI}O(O_2)$(ap-bhz)(MeOH)] **5**, [$Mo^{VI}O(O_2)$(ap-inh)(MeOH)] **6**, [$Mo^{VI}O(O_2)$(ap-nah)(MeOH)] **7** and [$Mo^{VI}O(O_2)$(ap-fah)(MeOH)] **8** have been prepared from potential tridentate hydrazones of 4-acetyl-3-methyl-1-phenyl-5-pyrazolone, H_2ap-bhz **I**, H_2ap-inh **II**, H_2ap-nah **III** and H_2ap-fah **IV** and characterized. Single crystal X-ray study of two $Mo^{VI}O_2$-complexes and two $Mo^{VI}O(O_2)$-complexes further confirm their structures. These complexes are very efficient homogenous catalyst precursors for the Hantzsch condensation reaction under solvent free condition. Reaction of methylacetoacetate, benzaldehyde and ammonium acetate gives two main products, dimethyl 2,6-dimethyl-4-phenyl-1,4-dihydropyridine-3,5-dicarboxylate (a) and dimethyl 2,6-dimethyl-4-phenylpyridine-3,5-dicarboxylate (b). Obtained conversion is highest at 40 ^oC with a : b selectivity ratio of ca. 10 : 90. This ratio changes to ca. 1 : 99 at 60 ^oC at the expense of lower conversion. The peroxido group on molybdenum complexes has no considerable effect and both type of complexes exhibit equally good conversion in the presence of H_2O_2. Reactivity of complex **3** with benzaldehyde in MeOH shows observable changes in its electronic spectra, suggesting its interaction with complex during catalytic action. The plausible role of peroxido intermediate complex in aromatization of dihydropyridine catalytically to the corresponding pyridine has also been suggested. It has been observed that solvent free catalytic method is better than doing Hantzsch reaction in solvent.

Acknowledgements

NS acknowledge MHRD fellowship and financial support through Indian Institute of Technology Roorkee, India.

References

1. O. D'Alessandro, Á. G. Sathicq, J. E. Sambeth, H. J. Thomas and G. P. Romanelli, *Catal. Comm.*, 2015, **60**, 65–69; *(b)* G. Swarnalatha, G. Prasanthi, N. Sirisha and C. M. Chetty, *Int. J. of ChemTech Res.* 2011, **3**, 75–89; *(c)* Y. Liu, J. Liu, X. Wang, T. Cheng and R. Li, *Tetrahedron*, 2013, **69**, 5242–5247 *(d)* H. Khabazzadeh, I. Sheikhshoaie, S. Saeid-Nia, *Transition Met. Chem.*, 2010, **35**, 125–127.

2. T. Tsuruo, H. Iida, M. Nojiri, S. Tsukagoshi and Y. Sakurai, *Cancer Research*, 1983, **43**, 2905–2910.
3. A. Krauze, S. Germane, O. Eberlins, I. Sturms, V. Klusa and G. Duburs, *Eur. J. of Med. Chem.*, 1999, **34**, 301–310.
4. X. Zhou, L. Zhang, E. Tseng, E. S. Ramsay, J. J. Schentag, R. A. Coburn and M. E. Morris, *Drug Metabolism Disposition*, 2005, **33**, 321–328.
5. R. W. Chapman, G. Danko and M. I. Siegels, *Pharmacology*, 1984, **29**, 282–291.
6. *(a)* W. J. Malaise and P. C. F. Mathias, *Diabetologia*, 1985, **28**, 153–156; *(b)* K. Aswin, K. Logaiya, P. N. Sudhan and S. S. Mansoor, *J. Taibah Univ. Sci.*, 2012, **6**, 1–9.
7. S. S. Mansoor, K. Aswin, K. Logaiya and S. P. N. Sudhan, *Arabian J. Chem.* http://dx.doi.org/10.1016/j.arabjc.2012.10.017.
8. *(a)* D. S. Bose, L. Fatima and H. B. Mereyala, *J. Org. Chem.*, 2003, **68**, 587–590; *(b)* V. L. Gein, M. I. Kazantseva and A. A. Kurbatova, Russ. *J. Org. Chem.*, 2011, **47**, 1123–1124; *(c)* K. Sirisha, D. Bikshapathi, G. Achaiah and V. M. Reddy, *Eur. J. Med. Chem.*, 2011, **46**, 1564–1571; *(d)* A. I. Matern, V. N. Charushin and O. N. Chupakhin, *Usp. Khim.*, 2007, **76**, 27–45; *(e)* A. M. Vijesh, A. M. Isloor, S. K. Peethambar, K. N. Shivananda, T. Arulmoli and N. A. Isloor, *Eur. J. Med. Chem.*, 2011, **46**, 5591–5597; *(f)* R. Pagadala, S. Maddila, V. D. B. C. Dasireddy and S. B. Jonnalagadda, *Catal. Commun.*, 2014, **45**, 148–152.
9. S. P. Chavan, S. W. Dantale, U. R. Kalkote, V. S. Jyothirmai and R. K. Kharul, *Synth. Commun.*, 1998, **28**, 2782–2792.
10. *(a)* F. Saikh, R. De and S. Ghosh, *Tetrahedron Lett.*, 2014, **55**, 6171–6174; *(b)* A. Saini, S. Kumar and J. S. Sandhu, *J. Sci. Ind. Res.*, 2008, **67**, 95–11; *(c)* L. Shen, S. Cao, J. Wu, J. Zhang, H. Li, N. Liu and X. Qian, *Green Chem.*, 2009, **11**, 1414–1420 *(d)* A. Debache, W. Ghalem, R. Boulcina, A. Belfaitah, S. Rhouati and B. Carboni, *Tetrahedron Lett.*, 2009, **50**, 5248–5250; *(e)* M. Litvic, M. Regovic, K. Šmic, M. Lovric and M. F. Litvic, *Bioorg. Med. Chem. Lett.*, 2012, **22**, 3676–3681; *(f)* M. Sharbatdaran, L. J. Foruzin, F. Farzaneh and M. M. Larijani, *C. R. Chimie*, 2013, **16,** 176–182; *(g)* M. Filipan-Litvic, M. Litvic and V. Vinkovic, *Bioorg. Med. Chem.*, 2008, **16**, 9276–9282.
11. *(a)* M. N. Esfahani, S. J. Hoseini, M. Montazerozohori, R. Mehrabi and H. Nasrabadi, *J. Mol. Catal. A: Chem.*, 2014, **382**, 99–105; *(b)* H. Mirzaei and A. Davoodnia, *Chin. J. Catal.*, 2012, **33**, 1502–1507.

12. *(a)* M. R. Maurya, S. Dhaka and F. Avecilla, *New J. Chem*., 2015, **39**, 2130–2139; *(b)* M. R. Maurya, N. Saini and F. Avecilla, *Inorg. Chem. Acta* 2015, **438**, 168–178.
13. *(a)* M.R. Maurya, *Curr. Org. Chem.*, 2012, **16**, 73–88; *(b)* S. Pasayat, S. P. Dash, S. Roy, R. Dinda, S. Dhaka, M. R. Maurya, W. Kaminsky, Y. P. Patil and M. Nethaji, *Polyhedron*, 2014, **67**, 1–10; *(c)* M. R. Maurya, S. Dhaka and F. Avecilla, *Polyhedron*, 2014, **67**, 145–159.
14. *(a)* M. Afsharpour, A. R. Mahjoub and M. M. Amini, *Appl. Catal. A:* Gen., 2007, **327**, 205–210; *(b)* M. M. Farahani, F. Farzaneh and M. Ghandi, *Catal. Commun.*, 2007, **8**, 6–10; *(c)* M. Bagherzadeh, R. Latifi, L. Tahsini, V. Amani, A. Ellern and L. K. Woo, *Polyhedron*, 2009, **28**, 2517–2521; *(d)* A. C. Coelho, M. Nolasco, S. S. Balula, M. M. Antunes, C. C. L. Pereira, F. A. A. Paz, A. A. Valente, M. Pillinger, P. R. Claro, J. Klinowski and I. S. Goncalves, *Inorg. Chem.*, 2011, **50**, 525–538; *(e)* A. Majumdar and S. Sarkar, *Coord. Chem. Rev.*, 2011, **255**, 1039–1054; *(f)* J. Pisk, D. Agustin, V. Vrdoljak and R. Poli, *Adv. Synth. Catal.*, 2011, **353**, 2910–2914; *(g)* R. D. Chakravarthy and D. K. Chand, *J. Chem. Sci*., 2011, **123**, 187–199. *(h)* J. Pisk, B. Prugovečki, D. M. Čalogović, R. Poli, D. Agustin and V. Vrdoljak, *Polyhedron*, 2012, **33**, 441–449; *(i)* M. E. Judmaier, C. Holzer, M. Volpe and N. C. M. Zanetti, *Inorg. Chem.*, 2012, **51**, 9956–9966; *(j)* S. Rayati, N. Rafiee and A. Wojtczak, *Inorg. Chim. Acta,* 2012, **386**, 27–35; *(k)* X. Lei and N. Chelamalla, *Polyhedron*, 2013, **49**, 244–251; *(l)* J. J. Boruah, S. P. Das, R. Borah, S. R. Gogoi and N. S. Islam, *Polyhedron*, 2013, **52**, 246–254.
15. G. J. J. Chen, J. W. McDonald and W. E. Newton, *Inorg. Chem.*, 1976, **15**, 2612–2615.
16. R. Verma, P. Chawla and S. K. Saraf, *Der. Pharmacia Sinica*, 2012, **3**, 546–555.
17. N. P. Moorjani, K. M. Vyas and R. N. Jadeja, *J. of Pure Appl. Sci.*, 2010, **18**, 68–72.
18. G. M. Sheldrick, *SADABS*, version 2.10, University of Göttingen, Germany, 2004.
19. G. M. Sheldrick, *Acta Crystallogr.*, *Sect. A*, 2008, **64**, 112–122.
20. N. K. Ngan, K. M. Lo and C. S. R. Wong, *Polyhedron*, 2011, **30**, 2922–2932.
21. *(a)* M. Herbert, F. Montilla, E. Alvarez and A. Galindo, *Dalton Trans.*, 2012, **41**, 6942–6956; *(b)* J. A. Brito, M. Gómez, G. Muller, H. Teruel, J-C. Clinet, E. Duñach and M. A. Maestro, *Eur. J. Inorg. Chem.*, 2004, **21**, 4278–4285.
22. M. R. Maurya, S. Dhaka and F. Avecilla, *Polyhedron*, 2014, **8**, 154–167.

23. *(a)* A. Syamal and M. R. Maurya, *Coord. Chem. Rev.*, 1989, **95**, 183–238; *(b)* R. Dinda, P. Sengupta, S. Ghosh, H. M. Figge and W. S. Sheldrick, *Dalton Trans.*, 2002, **23**, 4434–4439.
24. A. D. Westland, F. Haque and J. M. Bouchard, *Inorg. Chem.*, 1980, **19**, 2255–2259.
25. M. R. Maurya, N. Saini and F. Avecilla, *Polyhedron*, 2015, **90**, 221–232.
26. A. D. Keramidas, A. B. Papaioannou, A. Vlahos, T. A. Kabanos, G. Bonas, A. Makriyannis, C. P. Rapropoulou and A. Terzis, *Inorg. Chem.*, 1996, **35**, 357–367.

Table of Contents Synopsis

Study of temperature dependent three components dynamic covalent assembly via Hantzsch reaction catalyzed by dioxido- and oxidoperoxidomolybdenum(VI) complexes under solvent free condition

M.R. Maurya, N. Saini and F. Avecilla

Synthesis and characterization of dioxido- and oxidoperoxidomolybdenum(VI) complexes, and their catalytic potential for the Hantzsch type reaction under solvent free condition, giving corresponding dihydropyridine and pyridine, are reported.